PNNL-24996

Pacific Northwest
NATIONAL LABORATORY

Proudly Operated by Battelle Since 1965

Investigations into the Effect of Current Velocity on Amidoxime-Based Polymeric Uranium Adsorbent Performance

December 2015

Gary A Gill, Li-Jung Kuo, Jonathan Strivens, Jordana Wood and Nicholas Schlafer, Pacific Northwest National Laboratory, Marine Sciences Laboratory, Sequim, WA 98382

Costas Tsouris, Environmental Sciences Division, Oak Ridge National Laboratory, Oak Ridge, Tennessee 37831

Austin Ladshaw and Sotira Yiacoumi, Georgia Institute of Technology, Atlanta, Georgia 30332

U.S. DEPARTMENT OF ENERGY

Prepared for the U.S. Department of Energy under Contract DE-AC05-76RL01830

PACIFIC NORTHWEST NATIONAL LABORATORY
operated by
BATTELLE
for the
UNITED STATES DEPARTMENT OF ENERGY
under Contract DE-AC05-76RL01830

Printed in the United States of America

Available to DOE and DOE contractors from the
Office of Scientific and Technical Information,
P.O. Box 62, Oak Ridge, TN 37831-0062;
ph: (865) 576-8401
fax: (865) 576-5728
email: reports@adonis.osti.gov

Available to the public from the National Technical Information Service
5301 Shawnee Rd., Alexandria, VA 22312
ph: (800) 553-NTIS (6847)
email: orders@ntis.gov <http://www.ntis.gov/about/form.aspx>
Online ordering: http://www.ntis.gov

This document was printed on recycled paper.
(8/2010)

Investigations into the Effect of Current Velocity on Amidoxime-Based Polymeric Uranium Adsorbent Performance

Prepared for: U. S. Department of Energy, Office of Nuclear Energy, Fuel Cycle Research and Development Program, Fuel Resources Program

Prepared by: Gary A Gill, Li-Jung Kuo, Jonathan Strivens, Jordana Wood and Nicholas Schlafer, Pacific Northwest National Laboratory, Marine Sciences Laboratory Sequim, WA 98382

Costas Tsouris, Environmental Sciences Division, Oak Ridge National Laboratory, Oak Ridge, Tennessee 37831

Austin Ladshaw and Sotira Yiacoumi, Georgia Institute of Technology, Atlanta, Georgia, 30332

Milestone Number: M2FT-16PN030201042
Work Package Number: FT-16PN03020104
Milestone Due Date: 12-1-2015
U. S. DOE-NE Program Manager: Dr. Stephen Kung
Milestone Level: M2
PNNL ERICA Release Number: PNNL-24996

Prepared for
the U.S. Department of Energy
under Contract DE-AC05-76RL01830

Pacific Northwest National Laboratory
Richland, Washington 99352

Executive Summary

The Fuel Resources Program at the U.S. Department of Energy's (DOE), Office of Nuclear Energy (DOE-NE) is developing adsorbent technology to extract uranium from seawater. This technology is being developed to provide a sustainable and economically viable supply of uranium fuel for nuclear reactors (DOE, 2010). Among the key environmental variables to understand for adsorbent deployment in the coastal ocean is what effect flow-rates or linear velocity has on uranium adsorption capacity. The goal is to find a flow conditions that optimize uranium adsorption capacity in the shortest exposure time. Understanding these criteria will be critical in choosing a location for deployment of a marine adsorbent farm.

The objective of this study was to identify at what linear velocity the adsorption kinetics for uranium extraction starts to drop off due to limitations in mass transport of uranium to the surface of the adsorbent fibers. Two independent laboratory-based experimental approaches using flow-through columns and recirculating flumes for adsorbent exposure were used to assess the effect of flow-rate (linear velocity) on the kinetic uptake of uranium on amidoxime-based polymeric adsorbent material. Time series observations over a 56 day period were conducted with flow-through columns over a 35-fold range in linear velocity from 0.29 to 10.2 cm/s, while the flume study was conducted over a narrower 11-fold range, from 0.48 to 5.52 cm/s. These ranges were specifically chosen to focus on the lower end of oceanic currents and expand above and below the linear velocity of ~ 2.5 cm/s adopted for marine testing of adsorbent material at PNNL.

There was only a very small or perhaps no difference in uranium adsorption capacity as a function of the linear velocity for the seawater exposure using flow-through columns. At 56-days of exposure, the range in adsorption capacities varied from a low of 3.26 ± 0.18 g U/kg adsorbent at 0.73 cm/s, to a high of 3.74 ± 0.45 g U/kg adsorbent at 1.75 cm/s. Even the slowest linear velocity, 0.29 cm/s produced an adsorption capacity of 3.50 ± 0.36 g U/kg adsorbent. There were some notable relationships with linear velocity. The adsorbent exposed in the fastest linear velocity showed a more rapid initial uptake compared to the slowest linear velocity. The half saturation time for the slowest velocity (0.29 cm/s) was 64 ± 11 days, while the half-saturation time for the fastest velocity is 17 ± 1 day. The slowest exposure velocity predicts a saturation capacity of 7.48 ± 0.77 g U/kg adsorbent, while the fastest exposure velocity predicts a saturation capacity of 4.29 ± 0.10 g U/kg adsorbent based on one-site ligand saturation modelling.

The flow-through column studies at different linear velocities were subjected to analysis by applying five different kinetic and reaction-based modelling approaches to the time series data. Each of the models evaluated was able to describe the data sets fairly well and all would be suitable for modelling the time series data for flow-through column studies. Based on average Euclidian norms determined for the individual linear velocities, The one-site ligand saturation model had a slightly better mean Euclidian norm (1.46×10^{-3}), compared to the Langmuir,

Irreversible, and Reversible models (1.62×10^{-3}, 1.62×10^{-3}, and 1.60×10^{-3}, respectively). The model with the poorest fit as evidenced by a Euclidian norm of 2.35×10^{-3} was the diffusion model. Because adsorption of uranium from seawater with amidoxime-based adsorbents is known to be reaction controlled, a reaction-based model such as the Langmuir or Reversible Transition Mechanism model would be preferred. The one-site ligand saturation model is also appropriate as long as it is not utilized far outside of the parameterization window.

The seawater exposure studies as a function of linear velocity using a flume stand in marked contrast to the results obtained with the flow-through column exposures. The 56-day uranium adsorption capacity at a linear velocity of 0.48 cm/sec was 2.02 ± 1.08 g U/kg adsorbent, while the 56-day uranium adsorption capacity at a linear velocity of 5.52 cm/s was 4.31 ± 0.39 cm/s, more than a two-fold difference. There is a continual increase in the predicted 56-day uranium adsorption capacity moving from the slowest to the faster velocities until the linear velocity reaches 3.2 cm/s, where the 56-day adsorption capacities for the 3.2 and 5.5 cm/s linear velocities are nearly identical (4.27 ± 0.56 and 4.31 ± 0.39 g U/kg adsorbent, respectively). The other one-site ligand saturation modelling parameters also showed significant variation, but there was no clear trend with linear velocity. Predicted half-saturation times varied from 19 ± 4.6 days at a linear velocity of 1.40 cm/s to 69 ± 14 days at a linear velocity of 3.23 cm/s. Predicted saturation capacities varied between 3.28 ± 0.30 g U/kg adsorbent at a velocity of 1.40 cm/s and 9.51 ± 1.25 g U/kg adsorbent at a linear velocity of 3.23 cm/s.

The flume experiments predicted a significantly higher adsorption capacity at the two higher flume flow-rates (3.23 and 5.22 cm/s, respectively) than did the flow-through column studies. Since the adsorbent material that was used for these studies came from a common batch of braids, this implies that the discrepancy is most likely related to either bias's in the testing methods or the form factor of the adsorbent material (loose fibers vs. braided material) and not due to variations in the adsorption capacity of the material. A similar trend was also observed for the predicted 56-day adsorption capacity. The half-saturation times tended to be higher in the flume study, but for several linear velocities the half-saturation times predicted fell within the error of both measurement techniques.

Based on the 56-day performance of the braided adsorbent in mostly laminar flow, the kinetics of adsorption reach a maximal rate when the current velocity exceeds approximately 3 cm/s. If the adsorbent material is deployed in a turbulent flow or there is another deployment strategy to create agitation or movement of the deployed braids within the water column, this will likely promote maximal adsorption rates at even lower linear velocities.

Acknowledgments

We thank George Bonheyo, Tarang Khangaonkar, David Abrecht, and Kendall Gillies for critical reviews of the draft of this report.

Acronyms and Abbreviations

ICPMS	Inductively Coupled Plasma Mass Spectrometry
ICPOES	Inductively Coupled Plasma Optical Emission Spectrometry
MSL	Marine Sciences Laboratory
ORNL	Oak Ridge National Laboratory
OSLSM	One-Site Ligand Saturation Modelling
PNNL	Pacific Northwest National Laboratory

Contents

Executive Summary iii
Acknowledgments v
Acronyms and Abbreviations v
1.0 Objective 1
2.0 Background 1
2.1 Kinetic Modelling of Uranium Uptake by Amidoxime-based Polymeric Adsorbents 1
2.2 Oceanic Currents 2
3.0 Experimental Approach 2
3.1 PNNL Ambient Seawater Exposure Systems 3
3.1.1 Flow-through Column Ambient Seawater Exposure System 3
3.1.2 Flume Experiments 7
3.1.3 Turbulence in the Flume 11
3.1.4 Experimental Design for Flume Testing 11
3.2 ORNL Adsorbent Material 12
3.3 Analytical Methods 12
3.3.1 Determination of Uranium and Trace Elements on Adsorbent Materials 12
3.3.2 Determination of Uranium in Seawater 12
3.4 Water Quality Measurements 13
3.5 One-Site Ligand Saturation Modeling 13
4.0 Results and Discussion 14
4.1 Flow-Through Column Experiments 14
4.2 Analysis of Flow-rate Effects on Uranium Adsorption Kinetics from Seawater 20
4.2.1 Assumptions Made for Model Analysis 20
4.2.2 Kinetic Models Examined 21
4.2.3 Optimization Results 26
4.2.4 Model Comparison Discussion 31
4.2.5 Choice of Modelling Approaches 32
4.3 Flume Experiments 33
4.3.1 Uranium Time Series Measurements 33
4.4 Comparison of Flow-Through Column and Flume Exposure Results 36
4.5 Vanadium Competition 39
5.0 Summary and Conclusions 41
6.0 References 42

Figures

Figure 1. Layout and components of the seawater delivery and multi-port manifold system used for exposing uranium adsorbent materials in flow-through columns to filtered ambient seawater under controlled temperature and flow conditions. 4

Figure 2. Two, 24 port manifold systems (back to back) with flow-through columns attached.....5

Figure 3. Nominal one inch ID (2.28 cm actual diameter, left panel) and nominal 1.5 inch (3.99 cm actual, right panel) ID flow-through columns packed with ORNL AF1 adsorbent material for a flow-rate experiment. The adsorbent was partitioned into several small "clumps" and held in place with 5 mm glass beads.....6

Figure 4. Side view depiction of the recirculating flume system used for exposing braided adsorbent material to filtered or unfiltered natural seawater under controlled temperature and flow-rate (linear velocity) conditions. Six braided adsorbent materials are depicted within the flume. An external pump is used to recirculate seawater in the flume. The linear velocity in the flume is controlled by a restriction on the exit of the pump. Fresh seawater is fed into the flume using the seawater delivery system depicted in Figure 1. Seawater rises in the flume to the height of the overflow tube and then spills out at the same rate as it is introduced from the head tank. 9

Figure 5. Flumes used for studying the effect of linear velocity on adsorption performance. The flume on the left is the 8 ft. flume (Flume B) and the flume on the right is the 6 ft. flume (Flume C) that is described in Table 2. The recirculation pump for flume C is shown in the lower left side of the picture. The inlet for fresh seawater is introduced through the ½ inch poly tubing on the near side of the flumes.....10

Figure 6. Adsorbent braid attached to a short length of 1/4-inch diameter polyethylene tubing. The tubing end is inserted into a PVC block attached to the bottom of the flume, fixing the braid in the flume in the desired exposure position. 10

Figure 7. Baffle system consisting of 6 inch long by ½ inch diameter PVC tubing used to reduce turbulence in the flumes. The left hand picture shows the inlet side of the recirculated seawater for the 6 ft. flume, and the right hand picture shows the exit side of the baffles for the both the 6 ft (left) and 8ft. (right) flume. 11

Figure 8. Time series measurements of uranium adsorption capacity as a function of the linear velocity of the seawater exposure in flow-through columns. 15

Figure 9. Time series measurements of uranium adsorption capacity as a function of linear velocity. Data are these same as shown in Figure 8, but broken into three groups by linear velocity. Lines drawn through the data represent one-site ligand saturation modelling.....16

Figure 10. Time series measurements of adsorption capacity for the slowest (0.29 cm/s) and fastest (10.2 cm/s) linear velocities used in the flow-through column tests with the ORNL adsorbent AF1.....17

Figure 11. Adsorption capacity determined at different time points across a range in linear velocities using the ORNL AF1 adsorbent in flow-through column exposures, ...18

Figure 12. Variation in the uranium saturation capacity, B_{max} (top panel), Half-saturation time, K_d (middle panel), and 56-day uranium adsorption capacity (bottom panel) as a function of the linear velocity of the seawater exposure in a flow-through column exposure. The 0.73 cm/s data point, which appears anomalous, is indicated by an open circle.....19

Figure 13. Relationship between the optimum half-saturation constants and velocity for the one-site ligand saturation modelling. Note that the linear relationship has a poor fit to the data (r^2 = 0.316).....26

Figure 14. Relationship between optimum forward rate constant and linear velocity for the simple Langmuir modelling kinetics. 27
Figure 15. Relationship between optimum forward rate constant of the the second reaction and linear velocity of the seawater exposure....28
Figure 16. Relationship between optimum forward rate constant of the second reaction and linear velocity of the seawater exposure. 29
Figure 17. Relationship between optimum intraparticle diffusivity and linear velocity of the seawater exposure. 30
Figure 18. Adsorption uptake data at the various column linear velocities versus modelled using the Reversible Transitional Mechanism reaction-based model and the average optimum kinetic parameters reported in Table 8....33
Figure 19. Time series measurements of uranium adsorption capacity at a range of linear velocities using the ORNL AF1 braided adsorbent in a flume exposure. The lower three velocities were conducted in the 8 foot flume (Flume B) and the higher three velocities were conducted in the 6 ft flume (Flume C). 34
Figure 20. Comparison of the time series measurements of uranium adsorption capacity for the fastest linear velocity (5.52 cm/s) and the slowest linear velocity (0.48 cm/s) with exposure using the PNNL flume. The lines drawn through the data points represent one-site ligand saturation modelling. The modelling parameters are given in Table 9. 35
Figure 21. 56-day time series pictures of the ORNL AF1 adsorbent braids during exposure in the PNNL flume. The exposures are grouped in pairs with the slowest velocity on the left (0.48 cm/s) and the fastest velocity on the right (5.52 cm/s). The day of exposure is given by the number in the lower right hand side of the paired pictures. 37
Figure 22. Comprison of one-site ligand saturation modelling parameters as a function of linear velocity for exposures conducted using flow-through columns and flumes. 38
Figure 23. Time Series measurements of vanadium adsorption capacity as a function of the linear velocity of the exposure. The left panel is results obtained with the flow-through column exposure and the right panel is the results obtained for the flume exposure. The lines drawn through the data points represent one-site ligand saturation modelling. Only the fastest and the slowest modelling curves are shown for the flow-through column and flume exposures. .40
Figure 24. Time series measurements of the vanadium to uranium mass ratio for different linear velocities in the flow-through columns (left panel) and flume exposures (right panel). 40

Tables

Table 1. Linear velocity for nine time series flow-through column experiments using three different diameters of flow-through columns and flow-rates ranging between 100 and 700 mL/min....7
Table 2. Dimensions of the two flumes used for investigating the effect of linear velocity on adsorbent capacity with ORNL braided adsorbents....8
Table 3. Flume configuration and associated water recirculation and input fresh seawater flow-rates used to produce a range in linear velocities....12
Table 4. One-site ligand saturation modelling of the flow-through column studies on the effect of flow-rate (linear velocity) on adsorption capacity and performance. 17

Table 5. Summary of Optimized Parameters for the One-site Ligand Saturation Model. 26
Table 6. Summary of Optimized Parameters for the Langmuir Model 27
Table 7. Summary of Optimized Parameters for Irreversible Transition Mechanism Modelling ... 28
Table 8. Summary of Optimized Parameters for Reversible Transition Modelling 29
Table 9. Summary of Optimized Parameters for the Diffusion Kinetics Model..... 30
Table 10. One-site ligand saturation modelling of uranium adsorption capacity for the six time series data sets shown in Figure 13. 34

1.0 Objective

The Pacific Northwest National Laboratory (PNNL) has a level 2 milestone (M2FT-16PN030201042) due December 1, 2015 to: Complete the field modeling evaluation and laboratory column experiments and issue a report on the effect of flow rate (linear velocity) on adsorbent performance. As a preface to this level 2 milestone, PNNL produced a level 3 milestone (M3FT-15PN0310053), which described the experimental design for evaluation of current velocity on adsorbent performance.

The objective of this study is to identify at what linear velocity the adsorption kinetics for uranium extraction starts to drop off due to limitations in mass transport of uranium to the surface of the adsorbent fibers. This information will be critical in establishing an oceanic site with sufficient current velocity for optimal adsorbent extraction. This particular investigation is targeted at understanding the effect of lower end coastal currents (< 10 cm/s) on adsorption kinetics.

2.0 Background

The Fuel Resources Program at the U.S. Department of Energy's (DOE), Office of Nuclear Energy (DOE-NE) is developing adsorbent technology to extract uranium from seawater. This technology is being developed to provide a sustainable and economically viable supply of uranium fuel for nuclear reactors (DOE, 2010). A critical criterion to understand to optimize adsorbent performance in a marine deployment is what environmental conditions will be optimal for adsorbent performance. Among the key environmental variables to understand is what flow-rates or linear velocity is needed to optimize performance. This will be a key parameter in the choice of site selected for development of a marine adsorbent farm. Understanding the kinetic constraints on the uptake of uranium onto amidoxime-based adsorbents is key to this understanding.

2.1 Kinetic Modelling of Uranium Uptake by Amidoxime-based Polymeric Adsorbents

In previous modeling work, it was shown that, in batch kinetic experiments where the adsorbent fibers are fluidized in well mixed seawater, the complexation reaction of the uranyl ion with amidoxime ligand is the rate-limiting step of the overall uranium uptake (Costas Tsouris, personal communication). The reason that uranium adsorption is reaction limited is the competition of carbonate ions in the solution with the amidoxime ligand on the adsorbent in forming a complex with the uranyl ion. A kinetic model was developed to describe the batch kinetic experimental data. This model will be employed in this study to investigate the effect of seawater flowrate on uranium adsorption. Since the goal of the study is to determine the critical linear velocity below which the adsorption kinetics for uranium starts to drop off, experiments

will be conducted at flow regimes where diffusion around and inside the adsorbent fibers will be comparable to reaction kinetics. Thus, mass-transfer models have to be developed to also account for diffusion. Reaction kinetics and mass-transfer models will be coupled with a convective transport model in order to describe experimental data obtained in this study. Experimental data will be used to calibrate and validate the mass-transfer and reaction models. Subsequently, the models can be used to predict uranium uptake in realistic ocean deployment scenarios.

2.2 Oceanic Currents

Open ocean surface currents are primarily wind driven. The velocity of wind driven surface currents decreases rapidly with depth, reaching maximal depths of 100-150 meters. The depth of wind driven currents is controlled primarily by the temperature structure in the upper ocean. Wind driven surface currents move at about 2% of the wind speed (Gross, 1993). A wind blowing at 10 m/s (22.4 MPH) will produce a surface current of ~ 20 cm/s (0.45 MPH).

Boundary currents exist along continental margins, driven by the major open ocean gyre systems. The most notable are the Gulf Stream and the Kurishio, which are western boundary currents. Western boundary currents are narrow (<100 km), deep (~2km), and fast (100-300 cm/s). Eastern boundary currents are much slower (~10-30 cm/s), quite broad (~1000 km) and shallower (<500 m) than western boundary currents. The California Current, which flows south along the west coast of the U.S., is an example of an eastern boundary current.

Deployment of a farm of braided "kelp-like" adsorbent material will most likely occur in a nearshore coastal environment (< 500 m depth), rather than the open ocean, and lie within a boundary current region. Deployment in a western boundary current (i.e., the Florida current, which runs along the east coast of the U.S.) will be problematic as current speeds (1-3 m/s) would make fixed position deployment extremely difficult, if not impossible. Hence, the most likely deployment areas will be eastern boundary current areas where currents would make deployment feasible, and yet still have sufficient velocity for optimal adsorbent performance.

3.0 Experimental Approach

Two independent laboratory-based experimental approaches using flow-through columns and recirculating flumes for adsorbent exposure were used to assess the effect of flow-rate (linear velocity) on the kinetic uptake of uranium on amidoxime-based polymeric adsorbent material. The experimental design and conditions used for these experimental approaches were designed to overlap, allowing comparison of results.

3.1 PNNL Ambient Seawater Exposure Systems

Marine testing was conducted at the Marine Sciences Laboratory (MSL), a coastal based marine laboratory within PNNL, using ambient seawater from Sequim Bay, WA. The MSL has a seawater delivery system that can provide ambient seawater into a "wet laboratory" for scientific investigations. Ambient seawater is drawn by pump from a depth of ~10 m from Sequim Bay through a plastic pipe. Raw seawater is pumped directly into the laboratory for use. Filtered seawater is obtained by first passing raw seawater through an Arkal Spin Klin™ filter system (nominal pore size 40 µm) to remove large particles. The partially filtered seawater is then stored in a large volume (~ 3,500 gal) reservoir tank outside the laboratory. This seawater is gravity fed into the laboratory research facilities through PVC piping where it can be passed through additional filtration to remove finer particles if needed at the point of use. Two types of exposure systems were employed in this program: flow-through columns for testing of loose fibers and other loose materials and a recirculating water flume for testing of braided adsorbent material.

3.1.1 Flow-through Column Ambient Seawater Exposure System

Figure 1 shows a diagram of the seawater delivery and manifold system used to expose adsorbent materials to 0.45 µm filtered ambient seawater in flow-through columns. Figure 2 is a picture of the manifold with flow-through columns attached. Seawater from a large outside storage reservoir is fed sequentially through 5 µm and then 1 µm cellulose filters and then collected in a 180 L fiberglass reservoir tank referred to as a "head tank." Seawater in the head tank is heated to the desired temperature using a 10 kW all titanium immersion heater. Temperature-controlled (20 ± 1.5 °C) seawater is drawn from the head tank with a pump (non-metallic pump head), passed through a 0.35 to 0.45 µm polyethersulfone (Memtrex MP, GE Power and Water) or cellulose membrane cartridge filter and into the 24-port PVC manifold. Water that is not used to expose adsorbent material passes through the manifold and is returned to the head tank. Pressure (2-6 psi) in the manifold is controlled with a gate valve at the outlet of the manifold.

MSL has four separate 24-port manifolds, linked to three separate head tanks, permitting testing of 96 adsorbent materials in flow-through columns simultaneously. The flow-rate of seawater passing through the columns is grossly controlled by varying the seawater delivery pressure in the manifold and then fine scale flow adjustments using a needle valve placed on the outlet of each flow-through column. A turbine flow sensor (DFS-2W, Clark Solutions) is attached to the outlet tubing to monitor and record the flow through each column. The signals from the sensors are captured by a homemade instrument package operated with National Instruments LabView software, which displays in real time the flow-rate of each column on the manifold and records integrated flow-rate measurements in increments ranging from a few seconds to several hours.

The temperature of the seawater flowing through the exposure system was monitored and recorded at the outlet of columns using an Omega model RDXL4SD handheld meter equipped with a long lead and non-metallic temperature probe. The temperature was recorded every 5-10 minutes by attaching the meter to a laptop computer using data recording and storage software provided with the instrument.

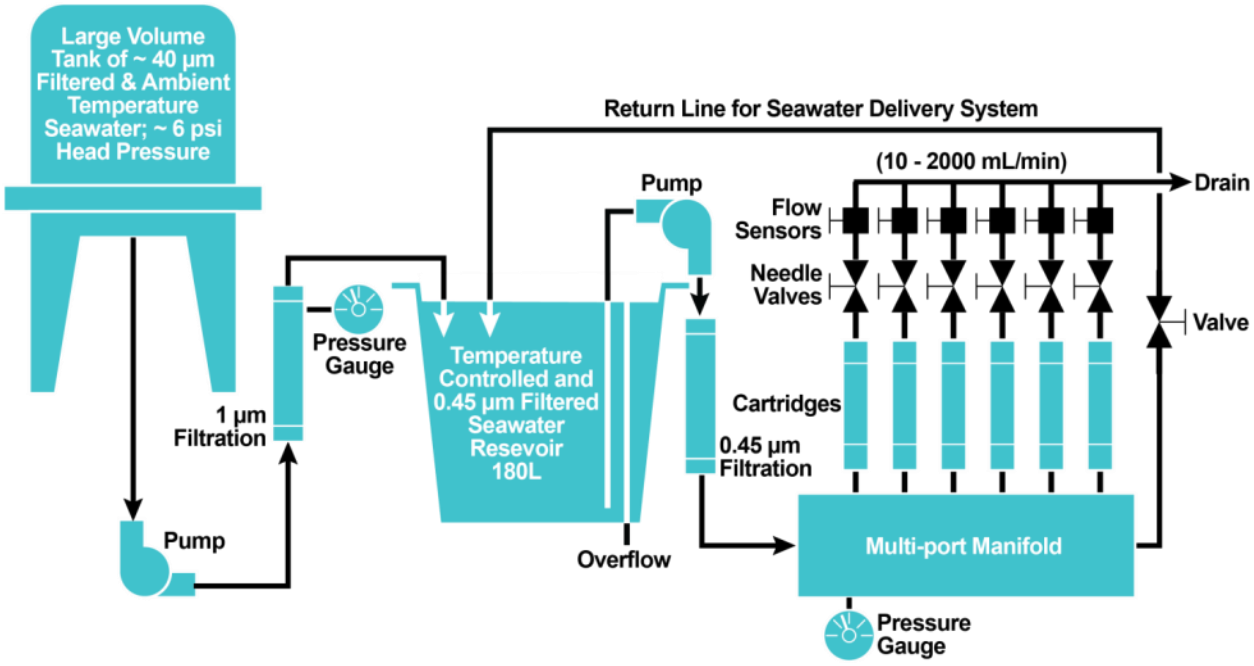

Figure 1. Layout and components of the seawater delivery and multi-port manifold system used for exposing uranium adsorbent materials in flow-through columns to filtered ambient seawater under controlled temperature and flow conditions.

Figure 2. Two, 24 port manifold systems (back to back) with flow-through columns attached.

3.1.1.1 Flow-Through Columns

The PNNL flow-through columns are constructed from all plastic components using commercially available materials. An example of a nominal 1-inch (2.28 cm actual) and a nominal 1.5 inch (3.99 cm actual) diameter column is shown in Figure 3. The column consists of a clear PVC tubing (Harvel Clear™ Rigid PVC Pipe) with threaded ends. Threaded PVC pipe fittings are used as end caps. Porous polyethylene sheets (Bel-Art Fritware®) with pore diameter of ~ 110 µm are used to construct frits. The frits are fitted inside the end caps and serve to contain the column contents. O-rings are placed on both sides of the frit and seal the end cap to the end of the column. Five mm diameter glass beads were used as column packing material to contain the adsorbent material.

Figure 3. Nominal one inch ID (2.28 cm actual diameter, left panel) and nominal 1.5 inch (3.99 cm actual, right panel) ID flow-through columns packed with ORNL AF1 adsorbent material for a flow-rate experiment. The adsorbent was partitioned into several small "clumps" and held in place with 5 mm glass beads

3.1.1.2 Packing of Columns

A critical feature in conducting the flow-rate experiments is how fibers are packed into the columns. Ideally, the fibers should be placed into the column in such a way that they have minimal contact with adjacent fibers. If the fibers are all in direct contact with each other (e.g., matted), then this arrangement could impede the contact between the seawater and the surface of the fiber, particularly for fibers on the interior of the matted adsorbent. For this reason, we mixed the fibers with the glass beads, attempting to distribute the fibers as evenly as possible throughout the column. In practice, however, the fibers were very difficult to separate and the best that could be achieved was to break the fibers into several small clumps and distribute the clumps throughout the column (see Figure 3). Glass wool packing normally used to hold fibers in place for most testing was avoided as a secondary packing material as it could result in significant fiber on fiber contact and adsorbent matting.

3.1.1.3 Column Flow-Rate, Linear Velocity, and Experimental Design

Linear velocities in the flow-through columns ranging between 0.3 and 10 cm/sec were achieved by using different diameter columns and seawater delivery flow-rates ranging between 100 and 700 mL/min (Table 1). The standard flow-rate used for determining adsorption capacity and adsorption kinetics were linear velocities between 2 and 2.5 cm/sec, which were achieved with a 1 inch ID column, packed with 5 mm glass beads, and a minimum flow-rate of 250

mL/minute (Kuo et al., 2015; Gill et al., 2015). The linear velocity in the column is a function of the internal column diameter, flow-rate and pore volume of the column packing:

$$\text{Linear velocity (cm/s)} = [(\text{column length, cm})(\text{flow-rate, L/s})]/(\text{pore volume, mL})$$

Where the pore volume is given by:

$$\text{Pore volume (mL)} = (\text{Porosity})(\pi)(\text{radius, cm})^2(\text{Column length, cm})$$

Porosity is defined as the fraction of the total volume that is not occupied by solid matter. Random packing of spherical grains greater than 100 µm in diameter have a porosity >0.399 and is independent of grain size. Independent measurements of the porosity of 3 and 5 mm glass beads packed into the 1 inch internal diameter (nominal size) PNNL column used for adsorption studies gave porosities of 0.425 and 0.454, respectively. A porosity of 0.454 was used for all calculations in this work.

Given in Table 1 below are the column diameters and flow-rates used to achieve a range in linear velocities between 0.29 and 10.4 cm/s. The column sizes were overlapped to achieve the range in an attempt to help identify any "column size" effects on the results. Each time series experiment was conducted for a total of 56 days, with 7 time points (0, 7, 14, 21, 28, 42 and 56 days) each. The final time point was replicated for a total of 8 samples per experiment.

Table 1. Linear velocity for nine time series flow-through column experiments using three different diameters of flow-through columns and flow-rates ranging between 100 and 700 mL/min.

Flow-Rate (mL/min)	Column Nominal Diameter (inches)	Column Measured Diameter (cm)	Linear Velocity (cm/s)
100	1.5	3.99	0.294
250	1.5	3.99	0.734
120	1.0	2.28	1.08
400	1.5	3.99	1.18
120	0.75	1.79	1.75
320	1.0	2.28	2.88
275	0.75	1.79	4.01
700	1.0	2.28	6.30
700	0.75	1.79	10.2

3.1.2 Flume Experiments

The Pacific Northwest National Laboratory has developed flow-through channels for conducting flume experiments under controlled temperature and flow-rate conditions. Different size pumps and flume dimensions are used to create a range in flow-rate (linear velocity). The seawater delivery system described previously provides fresh filtered seawater to the flume at desired temperatures and flow-rates up to 5 L/min.

3.1.2.1 Recirculating Flume Design and Operation

Two flumes constructed from darkened acrylic material with different dimensions were used for conducting exposure tests with braided adsorbent material under controlled temperature and flow-rate (linear velocity) conditions (Table 2). Darkened acrylic material was used to limit biological growth. The specific dimensions were selected to allow for reproducing a range in linear velocities that one might encounter in a coastal marine environment (< 10 cm/s). The target linear velocity around which the flows were varied was 2 cm/sec, which is approximately the linear velocity being used for testing with flow-through columns at PNNL.

Table 2. Dimensions of the two flumes used for investigating the effect of linear velocity on adsorbent capacity with ORNL braided adsorbents

Flume	Internal Length (ft)	Internal Length (cm)	Internal Width (inches)	Internal Width (cm)	Target Internal Depth (inches)	Target Internal Depth (cm)	Cross Sectional Area (cm^2)	Volume (L)
B	8	244	8	20.3	9.25	23.5	477	116
C	6	183	6	15.2	7	17.8	271	50

Shown in Figure 4 is a cross sectional view of the flume design illustrating the recirculation system and seawater inlet. A picture of the two flumes is shown in Figure 5. Fresh seawater is fed into the flume at flow-rates up to 5 L/min using the seawater manifold delivery system depicted in Figure 1. A tubing line was run from one or more of the manifold ports directly into the flume to achieve the desired seawater delivery rates. The rate of fresh seawater delivery was controlled using a needle valve mounted on one or more ports in the manifold. The height of water in the flume is controlled by the height of the stand pipe, which can be varied between approximately 7 and 11 inches (18-28 cm). Water within the flume rises until it reaches the height of the standpipe and then spills out of the flume through the standpipe. Raising or lowering the water height changes the cross sectional area of the water in the flume, which in turn is a means to control the linear velocity in the flume.

Braided adsorbents were placed into the flumes for exposure by attaching them to a short length of ¼ inch polyethylene tubing with cable ties and inserting one end of the tubing into a small block mounted on the bottom of the flume into which a ¼ inch hole has been drilled (Figure 6).

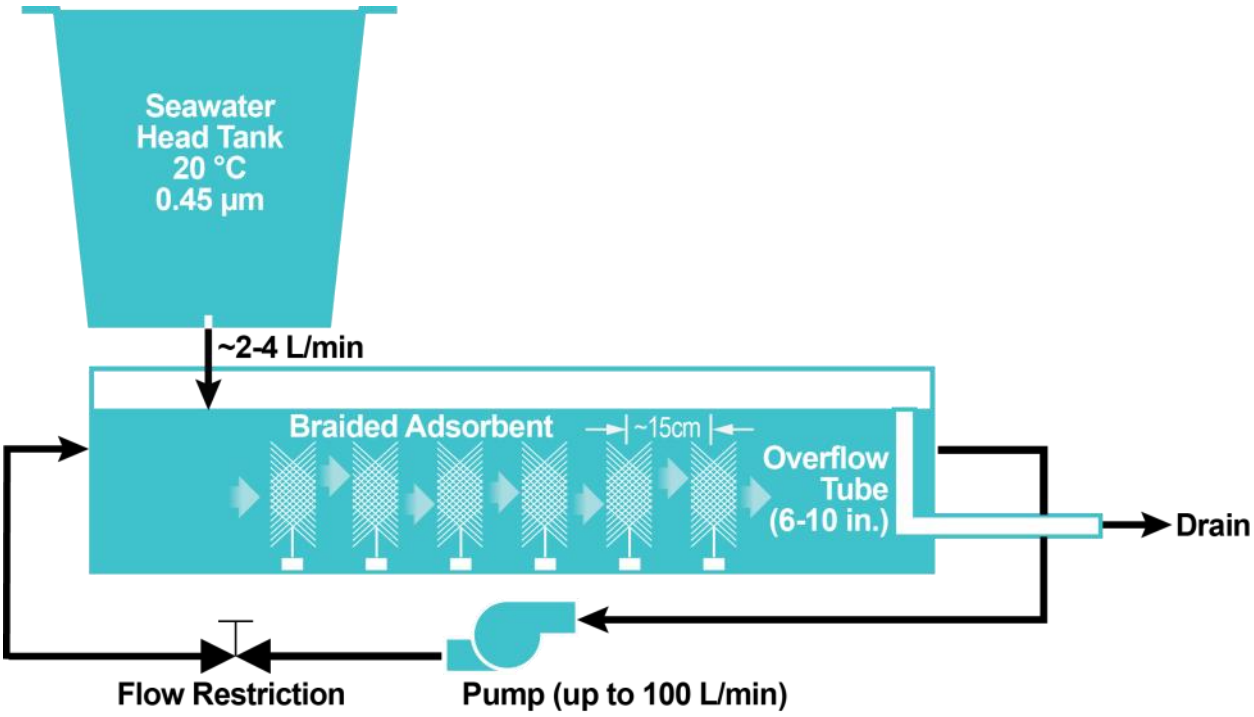

Figure 4. Side view depiction of the recirculating flume system used for exposing braided adsorbent material to filtered or unfiltered natural seawater under controlled temperature and flow-rate (linear velocity) conditions. Six braided adsorbent materials are depicted within the flume. An external pump is used to recirculate seawater in the flume. The linear velocity in the flume is controlled by a restriction on the exit of the pump. Fresh seawater is fed into the flume using the seawater delivery system depicted in Figure 1. Seawater rises in the flume to the height of the overflow tube and then spills out at the same rate as it is introduced from the head tank.

Controlled water flow within the flume is accomplished by recirculating the seawater within the flume using a Finish Thompson (models DB 5, DB6, and DB6H) centrifugal water pump (Figure 4). The pump head is non-metallic to minimize contamination concerns. Precise control of flow-rate/linear velocity was achieved by putting a flow restriction (globe valve) at the outlet of the pump. The flow-rate in the recirculating water was continuously monitored by placing a flow meter (Omega) in the line between the flume outlet and pump inlet. The linear velocity in the tank was determined using the cross sectional area of the tank and the recirculation flow-rate. For example, a linear velocity of 5.52 cm/s was achieved in the 6 foot (183 cm) flume with a 7 inch (17.8 cm) water height (cross sectional area of 271 cm^2) using the highest capacity pump and setting the flow-rate to 23 GPM (87 L/min). There is a slight increase in linear velocity (~3%) due to the fresh seawater in flow of 2.5 L/min, but it is small relative to the recirculation flow of 87 L/min.

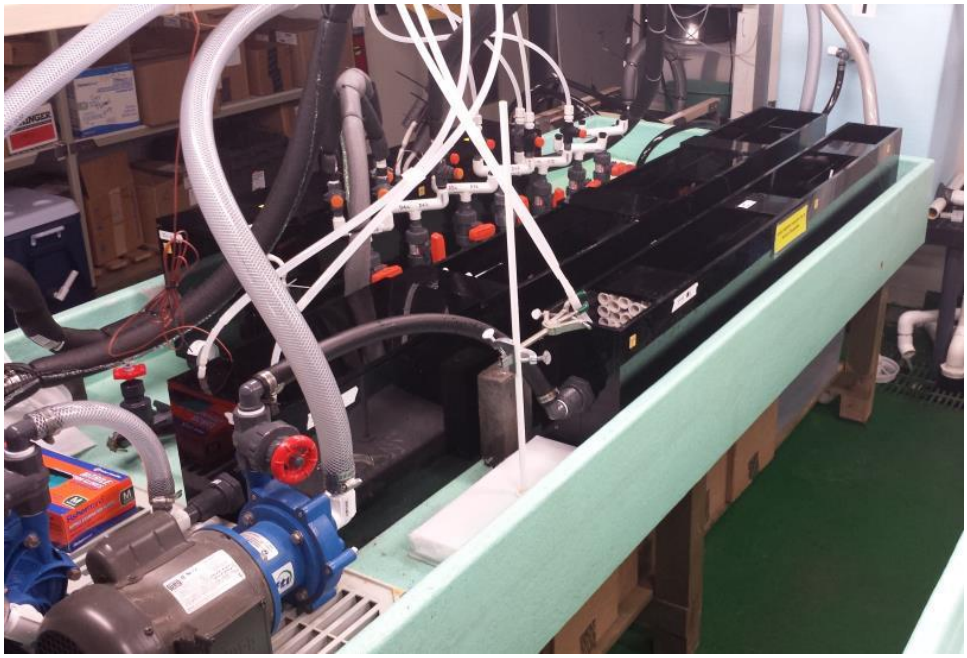

Figure 5. Flumes used for studying the effect of linear velocity on adsorption performance. The flume on the left is the 8 ft. flume (Flume B) and the flume on the right is the 6 ft. flume (Flume C) that is described in Table 2. The recirculation pump for flume C is shown in the lower left side of the picture. The inlet for fresh seawater is introduced through the ½ inch poly tubing on the near side of the flumes

Figure 6. Adsorbent braid attached to a short length of 1/4-inch diameter polyethylene tubing. The tubing end is inserted into a PVC block attached to the bottom of the flume, fixing the braid in the flume in the desired exposure position.

The rate at which fresh seawater is fed into the system and the internal volume of the flume controls the residence time of seawater in the system. For the above example with the 6 ft. flume, the water residence time is ~20 minutes. The time to recirculate water is much faster. At a recirculation flow rate of 87 L/min, the water in the flume is recirculated once every 24 seconds. For the lowest recirculation flow-rate (11 LPM), with the 8 foot flume, the flume water

residence time is 10 minutes. Hence, even at the lowest recirculation rate, the water in the flume is well mixed.

3.1.3 Turbulence in the Flume

At the end of the flume where the recirculated water is introduced, the flow is highly turbulent. Within 2-3 feet, the turbulence diminishes rather dramatically. Near the exit of the flume the flow is much more laminar. For flow-rate studies, the water flow in the flume was made more laminar using a series of baffles, consisting of short lengths (~ 6 inches) of ½ inch PVC tubing that was added near the recirculation inlet side of the flume. In addition, the positioning of the adsorbent was near the recirculation exit side of the flume where the water flow was most laminar.

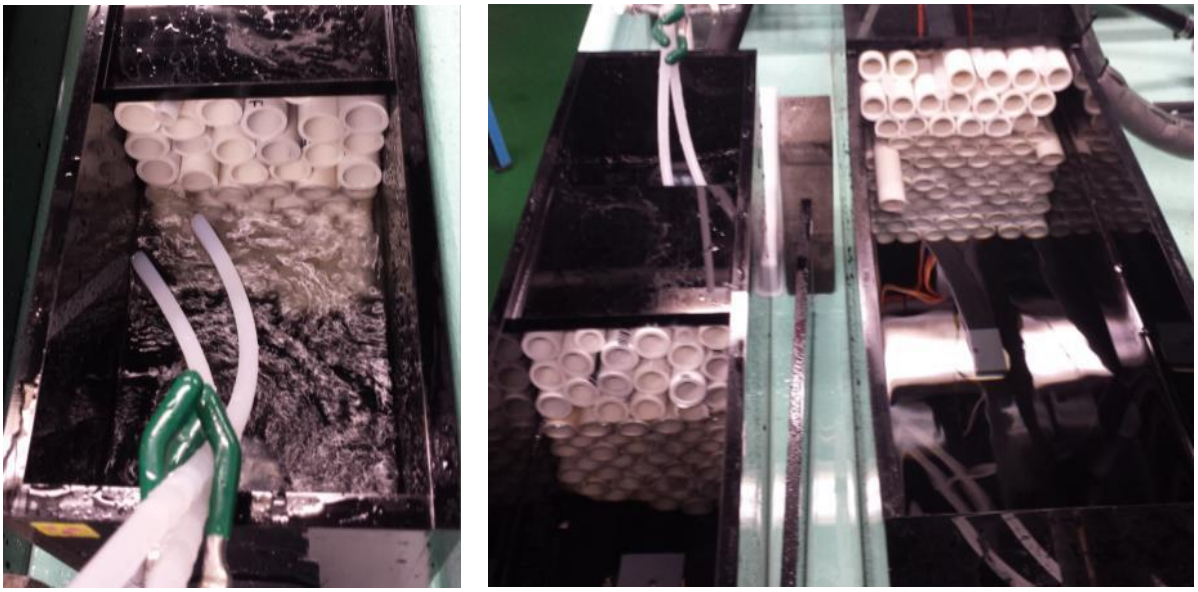

Figure 7. Baffle system consisting of 6 inch long by ½ inch diameter PVC tubing used to reduce turbulence in the flumes. The left hand picture shows the inlet side of the recirculated seawater for the 6 ft. flume, and the right hand picture shows the exit side of the baffles for the both the 6 ft. (left) and 8 ft. (right) flume.

3.1.4 Experimental Design for Flume Testing

Six independent flume experiments were conducted, each with a different linear velocity, ranging between 0.48 and 5.5 cm/s (Table 3). This range in linear velocities matches well with the range in linear velocities for the column studies (0.29 to 10.2 cm/s). Two exposures were conducted simultaneously, starting with experiments 1 and 6, then 2 and 5, and finally experiments 3 and 4. Flume B, which had the larger cross sectional area, was used for the slower linear velocities and Flume C, with the smaller cross-sectional area was used for the faster linear

velocities (Tables 2 and 3). Experiments consisted of 56 day time series exposures, with 8 sample time points (0, 7, 14, 21, 28, 35, 42 and 56 days). A replicate of the 21 day and 56 day sample time point was collected for a total of 10 samples per experiment.

Table 3. Flume configuration and associated water recirculation and input fresh seawater flow-rates used to produce a range in linear velocities.

Experiment	Flume Dimensions, (cm) (L x W x H)	Recirculation Rate (LPM)	Fresh Seawater Input Rate (LPM)	Linear Velocity (cm/s)
1	183 x 15 x 20	87.1	2.5	5.52
2	183 x 15 x 20	50.0	2.5	3.23
3	183 x 15 x 20	31.6	2.5	2.11
4	244 x 20 x 25	37.5	2.5	1.40
5	244 x 20 x 25	22.7	2.5	0.881
6	244 x 20 x 25	11.4	2.5	0.484

3.2 ORNL Adsorbent Material

The flow-rate tests were conducted with the ORNL AF1 formulation adsorbent provided by Chris Janke, which is described by Das et al. (2015) and Kuo et al (2015). All of the six braided adsorbent materials used for this study came from a common batch. The adsorbents were conditioned immediately before use with 0.44 M KOH for 1 hour at 80°C.

3.3 Analytical Methods

3.3.1 Determination of Uranium and Trace Elements on Adsorbent Materials

Adsorbent materials exposed to seawater were washed with deionized water to remove salts, and the monitoring the process with a conductivity meter. Samples were then dried at 80°C to a constant weight using a heated block (ModBlock™, CPI International). The dried fibers (50 to 100 mg) were weighed and then digested with 10 mL of a high-purity (Optima Grade, Fisher Scientific) 50% aqua regia acid mixture (3:1; hydrochloric acid: nitric acid) for 3 hours at 85°C on a hot block. Analysis of uranium and other trace elements was conducted using either a Perkin-Elmer 4300 inductively coupled plasma optical emission spectrometer or a Thermo Scientific ICap™ Q inductively coupled plasma mass spectrometer. Quantification with both instruments is based on standard calibration curves.

3.3.2 Determination of Uranium in Seawater

Determination of uranium in natural seawater samples was conducted using ICP-MS and either the method of standard addition calibrations or the samples were preconcentrated onto a

chelating ion exchange resin to minimize the seawater matrix, followed by acid elution with quantification against a standard calibration curve prepared using on-line pre-concentration (Wood et al., 2015).

Addition calibration is a variant of the standard additions method and is often used when all samples have a similar matrix. Instrumental calibration curves were prepared in Sequim Bay seawater that was diluted 20-fold with high purity deionized water and then spiked at 4 different concentration levels: 0.1, 0.2, 0.3, and 0.4 µg/L, along with a 2% nitric acid blank in diluted seawater. The seawater samples were then analyzed at 20-fold dilution with high purity deionized (DI) water and then quantified using the matrix matched additions calibration curve. The standard reference material CASS-5 (Nearshore seawater reference material for trace metals) available from the National Research Council Canada, which is certified for uranium (3.18 ± 0.10 µg/L), was also analyzed at a 20-fold dilution every 10 samples to verify the analytical results. The uranium recovery for the analysis of CASS-5 ranged from 93-99% (n=9). Duplicate analyses and matrix spikes were conducted with each batch of samples. The relative percent difference for duplicates ranged from 1-5%, and the recovery of matrix spikes ranged from 93-109% (n=11).

On-line pre-concentration of uranium was conducted using the seaFAST S2™ automated sample introduction system (Elemental Scientific) utilizing a seaFAST PFA chelation column packed with iminodiacetic acid chelating ion exchange resin (ESI, Seawater Concentrator Column CF-N-0200). Analytes were eluted off the column using 10% HNO3 and detected by ICPMS.

3.4 Water Quality Measurements

Salinity and pH measurements were conducted daily during the week. Salinity was determined using a handheld YSI salinometer. The pH was measured with a standard pH meter and probe that was calibrated weekly using NIST-traceable buffers.

3.5 One-Site Ligand Saturation Modeling

Measurements of the adsorption of uranium and other elements from seawater as a function of time onto the adsorbent materials were used to determine the adsorbent capacity and adsorption rate (kinetics) of uranium and other elements. Determination of adsorption capacity and kinetics was conducted using one-site ligand saturation modeling, which was parameterized using the software graphics program SigmaPlot©. The best-fit line representing the time series adsorption of uranium is given by:

$$u = \frac{\beta_{\max} t}{K_d + t} \tag{1}$$

Where u is uranium capacity (g U/kg adsorbent), t is exposure time (days), β_{max} is the adsorption capacity at saturation (g U/kg adsorbent), and K_d is the half-saturation time (days).

Prior to determination of adsorption capacity and kinetics, the individual capacity determinations were normalized to a salinity of 35 psu using simple proportional relationships. The ability to normalize the uranium data to a common salinity for comparison purposes is possible because there is a well-defined relationship between the 238-U concentration in seawater and salinity of 3.187 µg U/kg of seawater (Owens et al, 2011). This normalization removes the differences that result from exposures in seawater with varying salinity and hence uranium concentrations. This salinity normalization is also done for the other elements as well, but the normalization is less well defined for non-conservative elements in seawater.

4.0 Results and Discussion

4.1 Flow-Through Column Experiments

The nine time series flow-through column exposures at linear velocities ranging from 0.29 to 10.2 cm/s are depicted in Figure 8 and grouped by velocity with one-site ligand saturation modelling for the various linear velocities in Figure 9. One-site ligand saturation modelling of the nine flow-through column experiments is given in Table 4. Note that the data in Table 4 for the 0.73 cm/s linear velocity does not agree well with the data points above and below this value, and with the general trends in the data. While this experimental data point appears to be anomalous, there is no known reason to explain why it is anomalous and permit rejection.

Figure 8 suggests that there was only a modest difference in adsorption capacity as a function of the linear velocity of the seawater exposure. This was somewhat surprising, given the 35-fold range in linear velocity over which the experiment was conducted and the extremely slow velocities tested. Taking a closer look at the data, however, there are several trends that are apparent. Figure 10 shows a comparison between the adsorption capacity for the slowest (0.29 cm/s) and fastest (10.2 cm/s) linear velocity. The adsorbent exposed in the fastest linear velocity showed a more rapid initial uptake compared to the slowest linear velocity. This feature is also borne out in the one-site linear saturation modelling (Table 4). The half saturation time for the slowest velocity (0.29 cm/s) is 64 ± 11 days, while the half-saturation time for the fastest velocity is 17 ± 1 day. Despite this significant difference in adsorption kinetics, both linear velocities reach comparable 56-day adsorption capacities, but the predicted saturation capacities are markedly different (Table 4). The slowest exposure velocity predicts a saturation capacity of 7.48 ± 0.77 g U/kg adsorbent, while the fastest exposure velocity predicts a saturation capacity of 4.29 ± 0.10 g U/kg adsorbent (Table 4).

An alternative approach for assessing adsorbent performance as a function of the linear velocity of the seawater exposure is to examine the adsorption capacity at different time points as a function of linear velocity (Figure 11). Notice that the adsorption capacity determined at times

points less than 28 days of exposure varies significantly with the linear velocity of the seawater exposure. However, after 28 days of exposure, the linear velocity used for the exposure plays a less significant role in the determination of the adsorption capacity. This treatment also supports the previous observation that slower linear velocities result in slower initial adsorption kinetics, but that after 28 days of exposure the adsorption kinetics are similar for all linear velocities.

More detail on the relationship between the one-site ligand saturation modelling parameters (saturation capacity, half-saturation time, and calculated 56-day adsorption capacity) and the liner velocity of the seawater exposure is shown in Figure 12. In all three parameters, there is a decrease as the linear velocity of the seawater exposure increases.

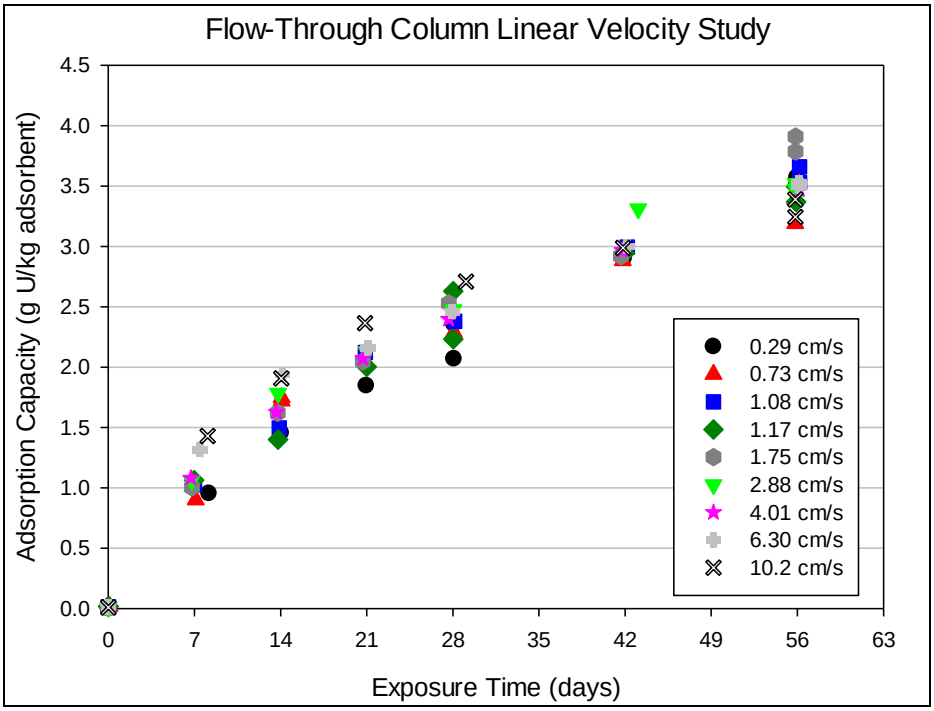

Figure 8. Time series measurements of uranium adsorption capacity as a function of the linear velocity of the seawater exposure in flow-through columns.

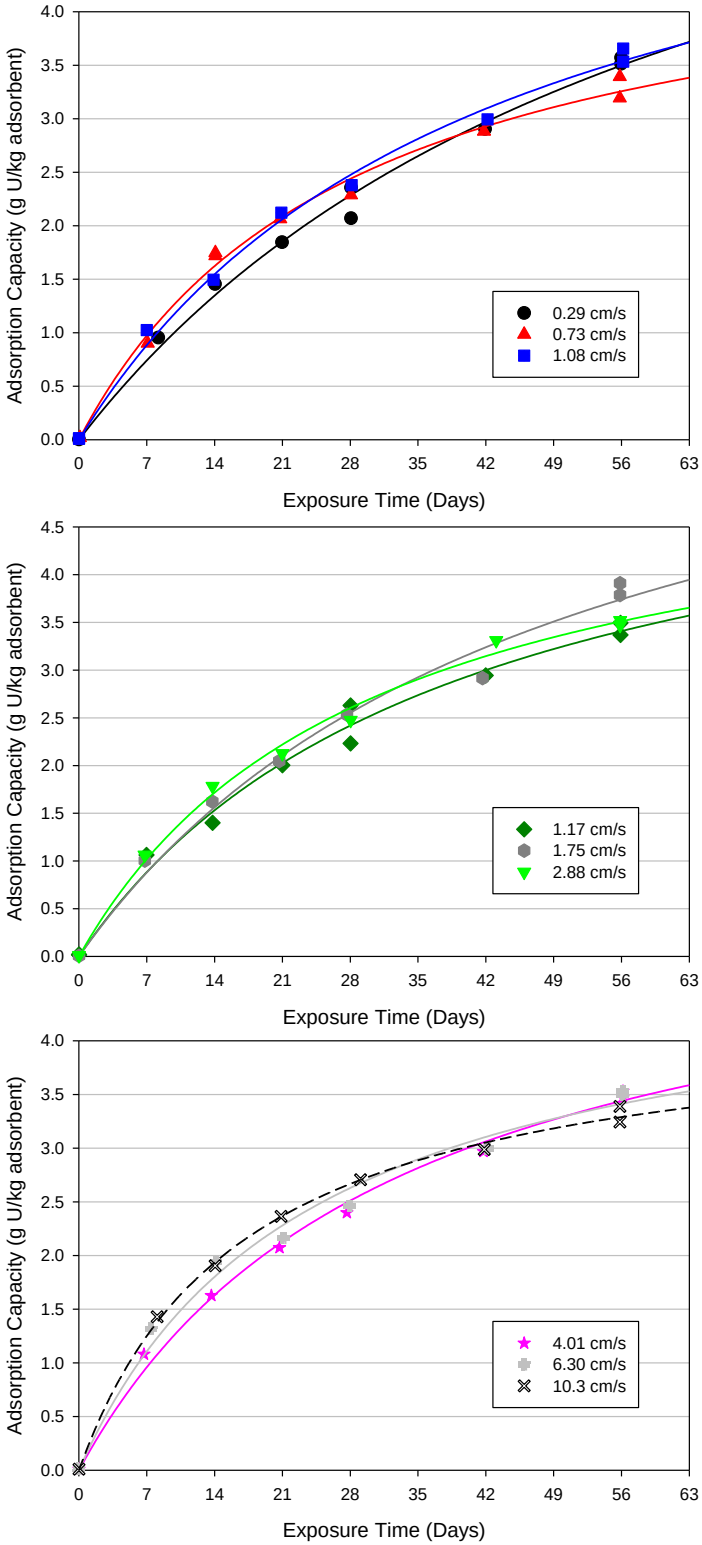

Figure 9. Time series measurements of uranium adsorption capacity as a function of linear velocity. Data are these same as shown in Figure 8, but broken into three groups by linear velocity. Lines drawn through the data represent one-site ligand saturation modelling.

Table 4. One-site ligand saturation modelling of the flow-through column studies on the effect of flow-rate (linear velocity) on adsorption capacity and performance.

Linear Velocity (cm/s)	Saturation Capacity[1,2], B_{max} (g U/kg Adsorbent)	Half-Saturation Time[1,2], K_d (days)	56 Day Adsorption Capacity[1,2] (g U/kg Adsorption)
0.29	7.48 ± 0.77	63.7 ± 10.6	3.50 ± 0.36
0.73	4.90 ± 0.27	28.3 ± 3.5	3.26 ± 0.18
1.08	6.19 ± 0.40	42.1 ± 5.3	3.53 ± 0.23
1.17	5.77 ± 0.51	38.7 ± 6.7	3.41 ± 0.30
1.75	7.00 ± 0.84	48.8 ± 10.7	3.74 ± 0.45
2.88	5.39 ± 0.29	30.0 ± 3.5	3.51 ± 0.19
4.01	5.46 ± 0.30	32.8 ± 3.8	3.44 ± 0.19
6.30	4.86 ± 0.33	23.8 ± 3.9	3.41 ± 0.23
10.2	4.29 ± 0.10	17.0 ± 1.1	3.29 ± 0.08

[1] Determined using one-site ligand saturation modelling
[2] Normalized to a salinity of 35 psu

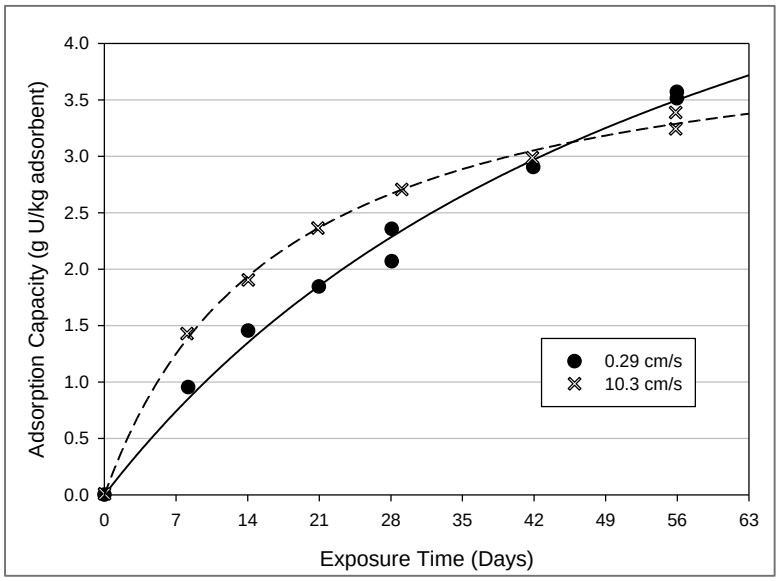

Figure 10. Time series measurements of adsorption capacity for the slowest (0.29 cm/s) and fastest (10.2 cm/s) linear velocities used in the flow-through column tests with the ORNL adsorbent AF1.

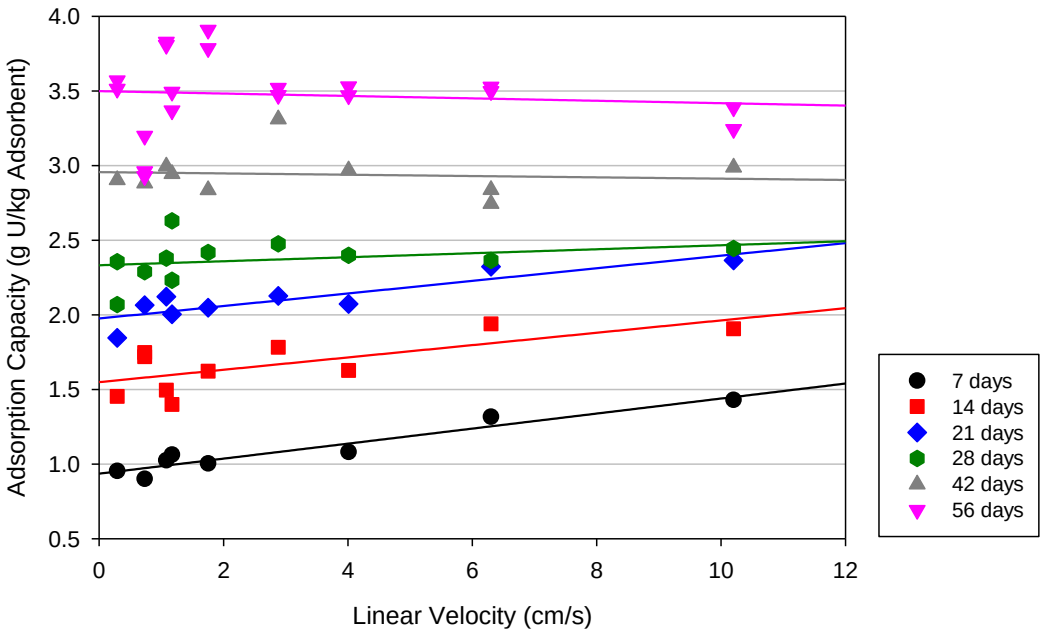

Figure 11. Adsorption capacity determined at different time points across a range in linear velocities using the ORNL AF1 adsorbent in flow-through column exposures,

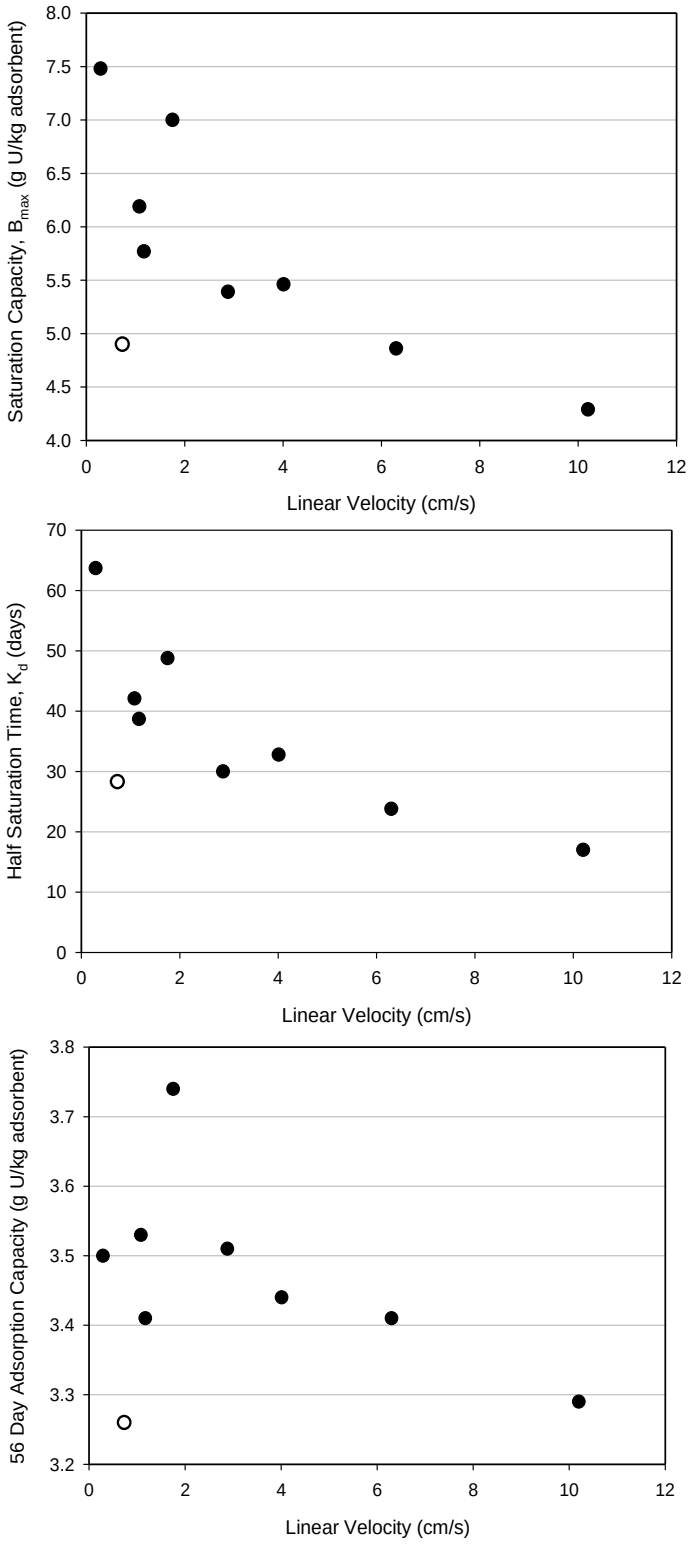

Figure 12. Variation in the uranium saturation capacity, B_{max} (top panel), Half-saturation time, K_d (middle panel), and 56-day uranium adsorption capacity (bottom panel) as a function of the linear velocity of the seawater exposure in a flow-through column exposure. The 0.73 cm/s data point, which appears anomalous, is indicated by an open circle.

4.2 Analysis of Flow-rate Effects on Uranium Adsorption Kinetics from Seawater

The flow-through column studies at different linear velocities were subjected to analysis by applying five different kinetic and reaction-based modelling approaches to the time series data. The suitability of the various modelling approaches was evaluated by taking the Euclidean norm of the residuals of the model predictions and the experimental data for each set (equation 2).

$$\|x\| = \sqrt{x_1^2 + x_2^2 + \cdots + x_n^2} \; for \; x \in \mathbb{R}^n. \tag{2}$$

The consistently changing system parameter throughout exposure testing was the flow rate of seawater through the columns. Changing the flow rate changes the linear velocity that the adsorbents are exposed to. A major goal of this study was to observe and quantify how changes in the linear velocity affect the overall uptake kinetics of uranium. We expect to see faster overall kinetics as the velocity increases. This is because mass transfer parameters, such as interparticle dispersion and film mass transfer coefficient, are proportional to this operating condition. Theoretically, saturation capacities, equilibrium constants, and reaction kinetics are unaffected by changes in linear velocity.

4.2.1 Assumptions Made for Model Analysis

Before analyzing the data, an understanding of the limits of the analysis and the assumptions that need to be made about the system in question is required. First, because detailed information about the concentrations of species at the inlet and outlet of the columns does not exist, an assumption needs to be made that the concentration of species in solution remains relatively constant. Generally speaking, this is not a good assumption because it would violate the conservation of mass. However, we can justify this assumption as an approximation of the system by noting the following points. (i) The kinetics of adsorption is very slow and will therefore have a minor impact on the concentration of species in solution; (ii) The flow rates in the system are very high relative to the kinetics, so the rate at which the species in the solution are replenished will likely be faster than the rate at which they are removed via adsorption.

Another major assumption that must be made deals directly with the quantification of key aqueous species. Because there were measurements of the inlet concentration of uranium during the experiment, we are able to assign a representative concentration for modelling purposes of 2.8 ppb (11.8 nmol/L). This is extremely important because the adsorption reaction is directly related to the concentration, and speciation, of the uranium in seawater. Further, we assume that the concentration of uranium remains constant in time, but also constant from experiment to experiment and that the chemical speciation of uranium, or any other adsorbing species, does not play a role in the kinetics. The representative value of uranium we will use here is 2.8 ppb (11.8 nmol/L).

4.2.2 Kinetic Models Examined

4.2.2.1 The One-Site Ligand Saturation Model

The one-site ligand saturation model (OSLSM) is a two parameter, empirical model that models absorption capacity, q(t), a function of time (equation 3). The OSLSM is the primary modelling tool currently used by PNNL to characterize uranium adsorption capacity as a function of time. Parameters of this model include a saturation capacity (q_{max}) and a half-saturation time (K_d). This model is frequently used in the biochemical field to model the saturation of a binding site (often referred to as a receptor) with a ligand (usually a small molecule). Binding is assumed to be a simple 1:1 association between ligand and receptor. This model assumes that the adsorbent will always reach its theoretical maximum saturation capacity if given enough time. Since saturation of adsorbent is slow, it is not clear how well this model will predict adsorption capacity outside of the specific operating conditions or time frame for which its parameters are optimized.

$$q(t) = q_{\max} \frac{t}{K_d + t} \tag{3}$$

4.2.2.2 Simple Langmuir Kinetics

A common approach often used is to represent adsorption as a site/ligand specific interaction between an aqueous species (A) and site/ligand (L) to produce an adsorption product (q), see the reaction scheme shown in Equation 4. The rate at which the adsorbed product changes with time is given by Equation 5. Applying this approach to uranium extraction allows us to represent the concentration of sites/ligands as the difference between some maximum value of sites/ligands (q_{max}) and the concentration of those sites already occupied, Equation 6.

$$A + L \Leftrightarrow q \tag{4}$$

$$\frac{dq}{dt} = k_1 \cdot A \cdot L - k_{-1} \cdot q \tag{5}$$

$$L = q_{\max} - q \tag{6}$$

Assuming that the concentration of species in solution is relatively constant, it is possible to formulate an analytical solution to this differential equation (equations 7 through 9). This expression includes three parameters: (i) q_{max} – maximum saturation capacity, (ii) k_1 – forward rate constant, and (iii) k_{-1} – reverse rate constant. Additionally, this model would allow use of an arbitrary initial condition for adsorption, represented by q_o. An equilibrium constant for this reaction can also be formed by the ratio of the forward and reverse rates ($K_1 = k_1/k_{-1}$). Both K_1 and q_{max} should not vary with the linear velocity.

$$q(t) = \frac{a}{b}\left(1 - \exp\left(-bt\right)\right) + q_o \exp\left(-bt\right) \tag{7}$$

$$a = k_1 \times A \times q_{\max} \tag{8}$$

$$b = k_1 \times A + k_{-1} \tag{9}$$

4.2.2.3 Irreversible Transitional Mechanism

Another modeling approach would be to consider a reaction mechanism that involves the formation of a temporary transition state product (q^*) before forming the final adsorbed species (q). This approach is very similar to the Michaelis-Menten kinetic model for catalysis in biological systems. To create this model, it is necessary to modify and add to the Langmuir reaction of equation 4 to form equation 10 below. This mechanism combines a two-step process by which the intermediate product (q^*) is formed by a reversible Langmuir-type reaction, followed by the irreversible formation of the final product (q).

$$A + L \underset{}{\overset{1}{\longleftrightarrow}} q^* \xrightarrow{2} q \tag{10}$$

From this expression, the rate of adsorption, shown in equations 11 and 12, can be formulated. A ligand-site balance can be enforced, as before, except now the total available ligand concentration is also a function of q* (equation 13). The end result is a coupled system of ordinary differential equations in q and q*. However, with a series of clever substitutions, q* can be decoupled from q in equation 10 and the problem can be solved analytically.

$$\frac{dq}{dt} = k_2 \cdot q^* \tag{11}$$

$$\frac{dq^*}{dt} = k_1 \times A \times L - k_{-1} \times q^* - k_2 \times q^* \tag{12}$$

$$L = q_{\max} - q - q^* \tag{13}$$

To solve this system, we must first go back to our earlier assumption about the concentration of uranium being constant in the system. Using this information, we can formulate the rate expression for the change in the adsorbate (A) with time and set that function to zero (equation 14). We can then solve that equation for L and substitute that expression into equation 13 above, which gives us an expression for q* as a function of only q and the associated constants (equation 15).

$$\frac{dA}{dt} = 0 = k_{-1} \times q^* - k_1 \times A \times L \quad \Rightarrow \quad L = \frac{k_{-1}}{k_1 \times A} q^* \tag{14}$$

$$q^* = \frac{q_{max} - q}{\left(\frac{k_{-1}}{k_1 \times A} + 1\right)} \tag{15}$$

We can now substitute equation 15 into equation 13 and integrate the uncoupled ordinary differential equation to obtain an analytical solution (equations 16 and 17). This expression involves four parameters: (i) q_{max} – maximum saturation capacity, (ii) k_1 – forward rate constant for first reaction, (iii) k_{-1} – reverse rate constant for first reaction, and (iv) k_2 – forward rate constant for second reaction. Similar to the Langmuir model, this expression includes an equilibrium constant ($K_1 = k_1/k_{-1}$) and maximum saturation capacity (q_{max}) that should not change with the linear velocity.

$$q(t) = q_{max}\left(1 - \exp\left(-k_2 t / a\right)\right) + q_o \exp\left(-k_2 t / a\right) \tag{16}$$

$$a = \frac{k_{-1}}{k_1 \times A} + 1 \tag{17}$$

4.2.2.4 Reversible Transitional Mechanism

An alternative to the previous model would be to consider a reversible secondary reaction step, as opposed to the irreversible case (equation 18). This formulation would change our rate expression for adsorption from equation 10 to equation 18 below. For this coupled system of differential equations, we can use many of the same substitution tricks as before to obtain an analytical solution (equations 19 through 21). Note that the derivation steps for arriving at this expression will not be provided here, since most steps are identical to before.

$$A + L \xleftrightarrow{1} q^* \xleftrightarrow{2} q \tag{18}$$

$$\frac{dq}{dt} = k_2 \times q^* - k_{-2} \times q \tag{19}$$

$$q(t) = \frac{k_2}{a \times b} q_{max}\left(1 - \exp\left(-bt\right)\right) + q_o \exp\left(-bt\right) \tag{20}$$

$$a = \frac{k_{-1}}{k_1 \times A} + 1 \tag{21}$$

$$b = \frac{k_2}{a} + k_{-2} \tag{22}$$

This model uses five parameters: (i) q_{max} – maximum saturation capacity, (ii) k_1 – forward rate constant for first reaction, (iii) k_{-1} – reverse rate constant for first reaction, (iv) k_2 – forward rate constant for second reaction, and (v) k_{-2} – reverse rate constant for the second reaction. Four of those parameters can be combined to form two equilibrium constants for the two reactions, $K_1 = k_1/k_{-1}$ and $K_2 = k_2/k_{-2}$. Those equilibrium constants, as well as the saturation capacity (q_{max}), should not vary with the linear velocity.

4.2.2.5 Film and Fiber Diffusion Kinetics

The last model we will consider is a mass transfer model whose primary adsorption mechanisms are film mass transfer and intraparticle diffusion. It may seem paradoxical to use a transport model to try to describe a phenomenon that is reaction controlled in seawater, but the same could be said of trying to quantify the effect of a rate of physical transport on the reaction kinetics of adsorption. In theory, the linear velocity should have absolutely no impact on the rate constants of a reaction. These two parameters are mutually exclusive, i.e., increasing linear velocity cannot and will not have an effect on reaction rate constants. There is no physical or chemical basis for stating otherwise.

However, we do expect to see an increase in the overall rate of uptake of uranium by the adsorbents when the linear velocity is increased. This is because as the velocity increases, the rate at which aqueous uranium reaches an adsorbent, where the reaction occurs, allows the reaction to proceed faster because there is more uranium to react with. However, since we do not have any breakthrough data for aqueous concentrations in the column, we cannot quantify how the linear velocity affects the interparticle dispersion in the system. Alternatively, we can quantify the relationship between linear velocity and the rate of film mass transfer through a dimensional analysis with the Sherwood (S), Schmidt, and Reynolds numbers (Tien, 1994).

Before we are able to perform any dimensional analysis, we must parameterize a mass transfer model based on the uranium uptake data we have to find the optimal intraparticle diffusivities (D) and film mass transfer coefficients (k). The model we will use is a cylindrical diffusion model with a Neumann boundary condition based on the rate of transfer of material across a film layer surrounding the fibers of radius (a) (equations 23 and 24). In this formulation of the problem, we replace what would have been the maximum saturation capacity (q_{max}) with the equilibrium adsorbed amount (q_e) that the fiber will reach based on the aqueous concentration in the system. Since we have already assumed that all aqueous concentrations are constant, and at the same level, for all experiments, then this q_e amount must also be a constant and have the same value for each data set.

$$r\frac{\partial q}{\partial t}=\frac{\partial}{\partial r}\left(rD\frac{\partial q}{\partial r}\right) \tag{23}$$

$$D\left.\frac{\partial q}{\partial r}\right|_{r=a}=k\left(q_e-q\right) \tag{24}$$

An analytical solution to the above partial differential equation can be formed if we further assume that the diffusivity (D) is a constant (Crank, 1975). If we also assume that the fiber initially contains no adsorbed uranium, we can integrate the solution over the domain of the fiber to form an expression for how the average adsorption in the fiber changes with time (equations 25 through 28). This is the form of the equation that we will use to compare against the kinetic rate data. It contains three parameters: (i) q_e – equilibrium adsorption, (ii) D – intraparticle diffusivity, and (iii) k – film mass transfer coefficient. In theory, only the film mass transfer coefficient should show any variance with the linear velocity for this model.

$$q(t)=q_e\left(1-\sum_{n=1}^{\infty}\frac{4S^2\exp\left(-\beta_n^2Dt/a^2\right)}{\beta_n^2\left(\beta_n^2+S^2\right)}\right) \tag{25}$$

$$S=\frac{ak}{D} \tag{26}$$

$$\beta_n\times J_1\left(\beta_n\right)-S\times J_0\left(\beta_n\right)=0 \tag{27}$$

$$J_a(x)=\sum_{m=0}^{\infty}\frac{\left(-1\right)^m}{m!\left(m+a\right)!}\left(\frac{x}{2}\right)^{2m+a} \tag{28}$$

Before proceeding further, it is important to note some of the limitations of using this particular model. The primary expression for adsorption with time (equation 24) involves a convergent infinite sum over all the roots (β_n) of the Bessel functions (J_1 and J_0) in equation 27. Those Bessel functions are themselves an infinite series of polynomials (equation 28). As such, it is mathematically impossible to exactly find all the roots of equation 27. Furthermore, as we will be performing an iterative optimization procedure using this function, changing the film mass transfer and intraparticle diffusion parameters, will actually change the values of the roots we are searching for.

In order to work around those complications and use this model, we will only seek the first six roots of the Bessel functions (Table 5.2: Crank, 1975). Those roots are a function of the Sherwood number (equation 26), which will be varied during the optimizations. Therefore, every time the Sherwood number changes, we will update those roots based on the set of known roots we have. This approach will allow us to approximate the first six values of β_n without needing additional computational mechanisms.

4.2.3 Optimization Results

4.2.3.1 The One-Site Ligand Saturation Model

Our analysis found that the optimal saturation capacity (q_{max}) for the entire set of data was approximately 0.0209 moles of uranium per kilogram of adsorbent (~4.98 g/kg). A table of the Euclidean norms of the data fits and half-saturation constants is provided below (Table 5). Note that the norms are the root-mean-squared errors for the differences between the model and the data for each set. Figure 13 shows the trend between the linear velocity in the system and the optimal half-saturation constant. As expected, a slight negative trend is observed, indicating that the increase in linear velocity resulted in a slight overall increase in the uptake rate, although the linear fit to the data is poor.

Table 5. Summary of Optimized Parameters for the One-site Ligand Saturation Model.

Velocity (cm/s)	Norm	K_d (hours)
0.29	1.53×10^{-3}	991
0.73	1.48×10^{-3}	953
1.08	1.03×10^{-3}	870
1.17	1.35×10^{-3}	942
1.75	1.88×10^{-3}	804
2.88	9.30×10^{-4}	808
4.01	8.26×10^{-4}	874
6.30	1.74×10^{-3}	837
10.20	2.42×10^{-3}	825
Maximum	2.42×10^{-3}	991
Average	1.46×10^{-3}	878

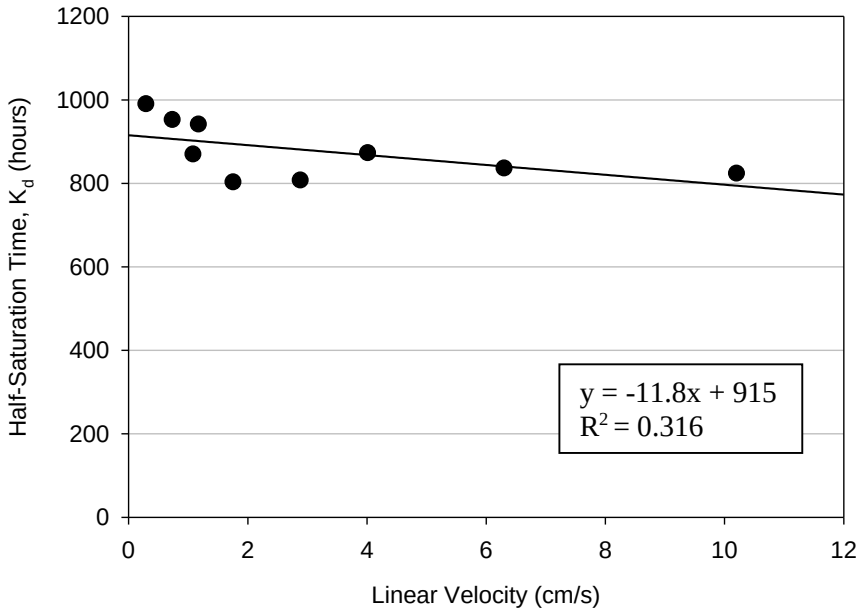

Figure 13. Relationship between the optimum half-saturation constants and velocity for the one-site ligand saturation modelling. Note that the linear relationship has a poor fit to the data (r^2 = 0.316)

4.2.3.2 Simple Langmuir Kinetics Modelling

For this model, our analysis found the optimal saturation capacity (q_{max}) to be approximately 0.0182 moles of uranium per kilogram of adsorbent (~4.34 g/kg). Additionally, we found that the equilibrium parameter (K_1) of this model to be approximately 3.72 x 10^8 L/mol (log K_1 = 8.57). Table 6 shows the list of norms and forward rate constants (k_1) with the linear velocity, and Figure 14 shows the relationship between velocity and k_1. This image shows a slightly positive correlation between the forward rate constant and system velocity, which is the expected trend since a larger forward rate constant would yield faster kinetics.

Table 6. Summary of Optimized Parameters for the Langmuir Model

Velocity (cm/s)	Norm	k_1 (L/mol/hr)
0.29	1.48 x 10^{-3}	8.66 x 10^4
0.73	1.76 x 10^{-3}	9.16 x 10^4
1.08	1.14 x 10^{-3}	9.90 x 10^4
1.17	1.44 x 10^{-3}	9.16 x 10^4
1.75	2.05 x 10^{-3}	1.07 x 10^5
2.88	1.07 x 10^{-3}	1.08 x 10^5
4.01	1.09 x 10^{-3}	9.91 x 10^4
6.30	2.00 x 10^{-3}	1.04 x 10^5
10.20	2.56 x 10^{-3}	1.08 x 10^5
Maximum	**2.56 x 10^{-3}**	**1.08 x 10^5**
Average	**1.62 x 10^{-3}**	**9.90 x 10^4**

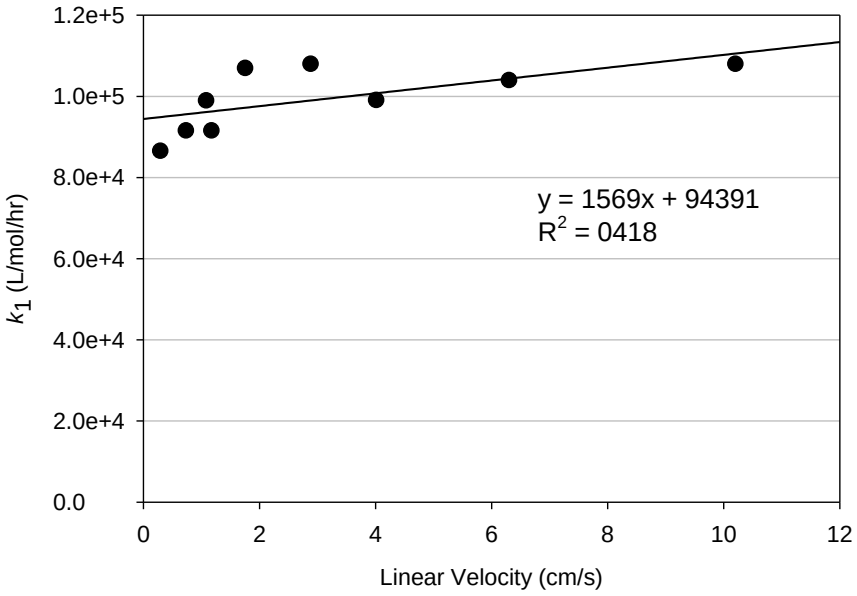

Figure 14. Relationship between optimum forward rate constant and linear velocity for the simple Langmuir modelling kinetics.

4.2.3.3 Irreversible Transitional Mechanism Modelling

For the irreversible model, our analysis found the optimal saturation capacity (q_{max}) to be approximately 0.0148 moles of uranium per kilogram of adsorbent (~3.53 g/kg). Additionally, we found that the equilibrium parameter (K_1) of this model to be approximately 1.08 x 10^4 L/mol (log K_1 = 4.03) and that the forward (k_1) and reverse (k_{-1}) rates for the first reaction remained constant at 593 L/mol/hr and 0.0549 hr^{-1}, respectively. Only the rate constant for the second reaction showed any variance with velocity. Table 7 shows the list of norms and forward rate constants of the second reaction (k_2) with the linear velocity, and Figure 15 shows the relationship between velocity and k_2. Again, this shows a positive correlation, as we would expect.

Table 7. Summary of Optimized Parameters for Irreversible Transition Mechanism Modelling

Velocity (cm/s)	Norm	k_2 (1/hr)
0.29	1.48 x 10^{-3}	9.85
0.73	1.76 x 10^{-3}	10.4
1.08	1.14 x 10^{-3}	11.3
1.17	1.44 x 10^{-3}	10.4
1.75	2.05 x 10^{-3}	12.1
2.88	1.07 x 10^{-3}	12.2
4.01	1.09 x 10^{-3}	11.3
6.30	2.00 x 10^{-3}	11.9
10.20	2.56 x 10^{-3}	12.2
Maximum	**2.56 x 10^{-3}**	**12.2**
Average	**1.62 x 10^{-3}**	**11.3**

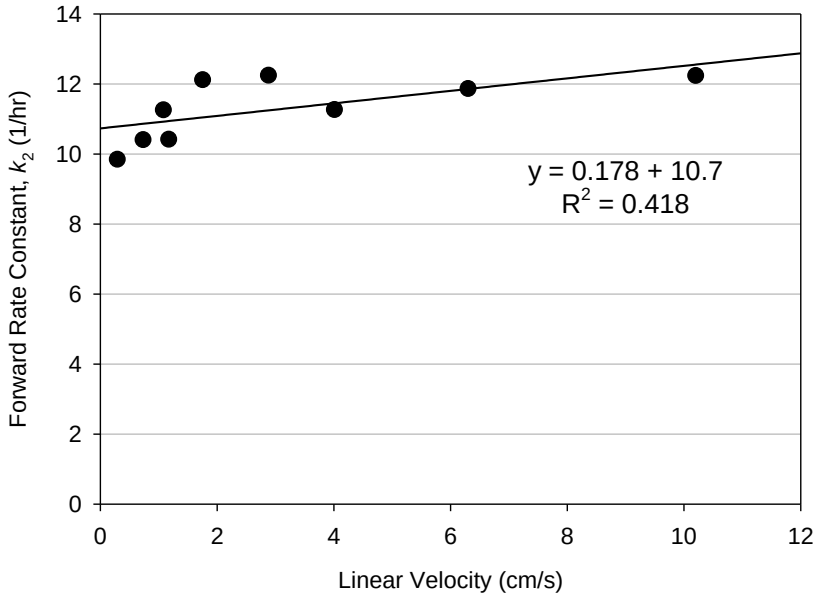

Figure 15. Relationship between optimum forward rate constant of the the second reaction and linear velocity of the seawater exposure

4.2.3.4 Reversible Transitional Mechanism

For the reversible transition mechanism, our analysis found the optimal saturation capacity (q_{max}) to be approximately 0.0235 moles of uranium per kilogram of adsorbent (~5.59 g/kg). Additionally, we found that the equilibrium parameters of the first and second reactions (K_1 and K_2) to be approximately 1.84 x 10^3 L/mol (logK_1 = 3.27) and 7.18 x 10^4 (log K_2 = 4.86), respectively. Similar to the irreversible model, the rate constants for the first reaction (k_1 and k_{-1}) were both found to be constant at 222.36 L/mol/hr and 0.1206 hr^{-1}, respectively. Only the rate constant for the second reaction showed any variance with velocity. Table 8 shows the list of norms and forward rate constants of the second reaction (k_2) with the linear velocity, and Figure 16 shows the relationship between velocity and k_2. Again, this shows a positive correlation, as we would expect.

Table 8. Summary of Optimized Parameters for Reversible Transition Modelling

Velocity (cm/s)	Norm	k_2 (1/hr)
0.29	1.65 x 10^{-3}	37.6
0.73	1.56 x 10^{-3}	40.0
1.08	1.30 x 10^{-3}	43.2
1.17	1.43 x 10^{-3}	39.9
1.75	2.27 x 10^{-3}	46.5
2.88	1.03 x 10^{-3}	47.3
4.01	1.08 x 10^{-3}	43.4
6.30	1.83 x 10^{-3}	45.9
10.20	2.24 x 10^{-3}	47.7
Maximum	**2.27** x 10^{-3}	**47.7**
Average	**1.60** x 10^{-3}	**43.4**

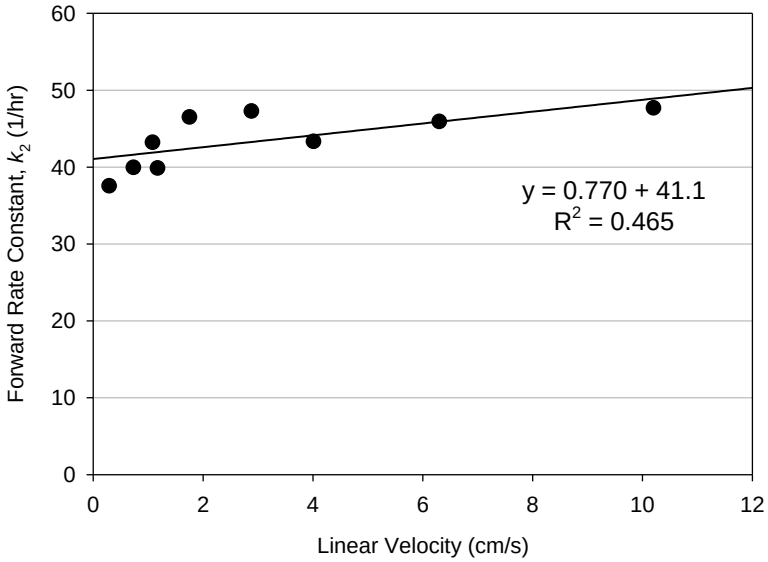

Figure 16. Relationship between optimum forward rate constant of the second reaction and linear velocity of the seawater exposure.

4.2.3.5 Film and Fiber Diffusion Kinetics Modelling

For the data analysis with the diffusion model, the radius of the fibers (a) was assumed to be roughly 76.5 μm, a nominal value given to us by ORNL. Our analysis found that the optimal equilibrium adsorption capacity (q_e) was approximately 0.0192 moles of uranium per kilogram of adsorbent (~4.56 g/kg). The more interesting and meaningful finding of this model analysis was that the results of the optimization found a remarkable lack of sensitivity that the model had to the film mass transfer parameter (k). We could change the value of that parameter from 1 to nearly ∞ without affecting the rate of the kinetics. Only the intraparticle diffusivity (D) had a noticeable effect on the uptake rate. Table 9 shows the optimum diffusivity parameters and norms of each optimization, and Figure 17 shows the correlations made between diffusivity and velocity.

Table 9. Summary of Optimized Parameters for the Diffusion Kinetics Model

Velocity (cm/s)	Norm	*D* (μm²/hr)
0.29	3.22×10^{-3}	0.4207
0.73	1.99×10^{-3}	0.4223
1.08	2.90×10^{-3}	0.4896
1.17	2.75×10^{-3}	0.4431
1.75	3.21×10^{-3}	0.5399
2.88	2.07×10^{-3}	0.5288
4.01	2.01×10^{-3}	0.4839
6.30	1.43×10^{-3}	0.5048
10.20	1.56×10^{-3}	0.5060
Maximum	**3.22×10^{-3}**	**0.5399**
Average	**2.35×10^{-3}**	**0.4850**

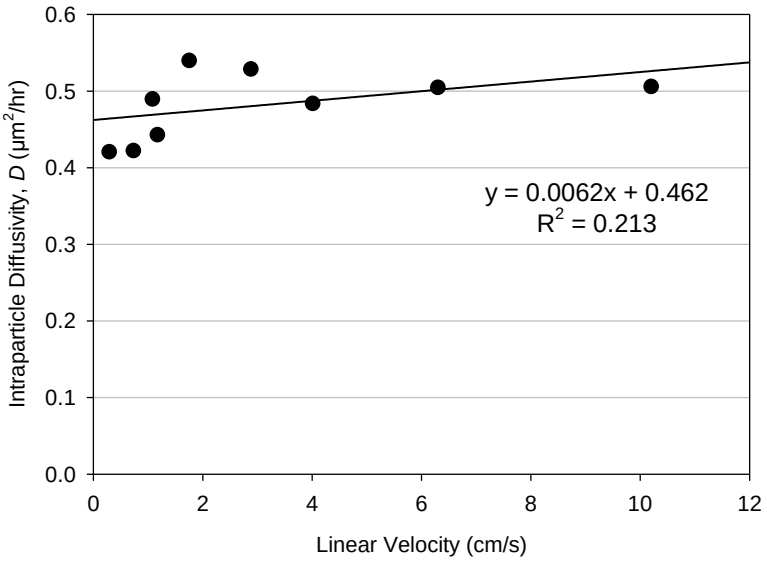

Figure 17. Relationship between optimum intraparticle diffusivity and linear velocity of the seawater exposure.

4.2.4 Adsorption Model Comparison Discussion

In theory, the rates of reaction and the intraparticle diffusivity should not be correlated with linear velocity. There is no physical, chemical, or theoretical basis for these supposed constants to change with flow rates. There is, however, expected to be more mechanical mixing in the system caused by an increase in the turbulence of the flow as more material is passed over the packed particles in the column. The increases in mechanical mixing will subsequently cause increases in the dispersion, or interparticle diffusivity, of aqueous phase constituents in the system. Additionally, by increasing both the flow and the dispersion in the system, the fibers will see higher concentrations, on average, of the respective aqueous phase constituents that they are taking up. Therefore, we expect the overall kinetics of the adsorption process to increase as the linear velocity increases, up to some finite limit.

Alternatively, there is a basis on which we can claim that the linear velocities in the system will have an effect on the film mass transfer rates of material across the initial barrier of the outside of the fiber. These correlations are accomplished by performing a dimensional analysis of the Sherwood, Schmidt, and Reynolds numbers. However, because our data analysis with the diffusion model showed no sensitivity to the film mass transfer parameter across all sets of data, we cannot perform that dimensional analysis.

The lack of sensitivity of the diffusion model to the film mass transfer coefficient indicates that the boundary condition of the problem (equation 24) does not contribute to controlling the overall uptake rate. Under this circumstance, the boundary behaves more like a Dirichlet, rather than a Neumann condition. We can also see this mathematically by rearranging equation 24 into equation 29 below. In this form, we can see that as the film mass transfer coefficient increases, the left side of the equation decreases. At the limit of infinite film mass transfer, the left side becomes zero, which enforces $q_e = q$ at the boundary, i.e., a Dirichlet boundary condition.

$$\frac{D}{k}\frac{\partial q}{\partial r}\bigg|_{r=a} = q_e - q \tag{29}$$

Going back to the reaction based models (2 through 4), recall that we had defined a maximum saturation capacity (q_{max}) to solve and produce solutions to the differential equations in terms of this parameter. In theory, this parameter should be representative of the absolute maximum moles of adsorbate that the fiber can take in. It is a constant associated with the fiber, not the system. However, since we did not know what this value was, we allowed it to be optimized for, so we could fit the models to the data. Each different model came up with a slightly different q_{max} value, but none of those optimum values are the true saturation capacities. Instead, they represent only the saturation capacity of the fiber in typical seawater. In reality, we

know that if we put these fibers in a solution spiked with much more uranium, then the observed adsorption would be higher than these optimized capacities.

4.2.5 Choice of Modelling Approaches

Each of the models evaluated was able to describe the data sets fairly well as is evident from the relatively small range in mean Euclidean norms observed (1.46×10^{-3} to 2.35×10^{-3}). The one-site ligand saturation model had a slightly better mean Euclidian norm (1.46×10^{-3}), compared to the Langmuir, Irreversible, and Reversible models (1.62×10^{-3}, 1.62×10^{-3}, and 1.60×10^{-3}, respectively). The model with the poorest fit as evidenced by a Euclidian norm of 2.35×10^{-3} was the diffusion model. However, the fitness of the data alone is not a good enough basis on which to choose an appropriate model. Previous work has already shown that the uptake of uranium from seawater onto amidoxime-base adsorbents is reaction controlled (Kim et al., 2013; Das et al., 2009). Based on this criteria, a reaction-based model such as the Langmuir or Reversible Transition Mechanism model would be preferred. The one-site ligand saturation model is also appropriate as long as it is not utilized far outside of the parameterization window.

Although a slight variation in the overall uptake rate of uranium is observed as the linear velocity increases, no attempt should be made to quantify this correlation in terms of changing reaction rate constants. There is no theoretical precedent to state otherwise. Therefore, each model examined should use the averages of the optimum parameters over all data sets, and not vary those parameters with the flow rate. Even by doing this, we can still obtain a reasonable approximation to the uptake rate of the fibers. Figure 18 below shows the Reversible Transition Mechanism model using the average optimum parameters against the entire kinetic data set.

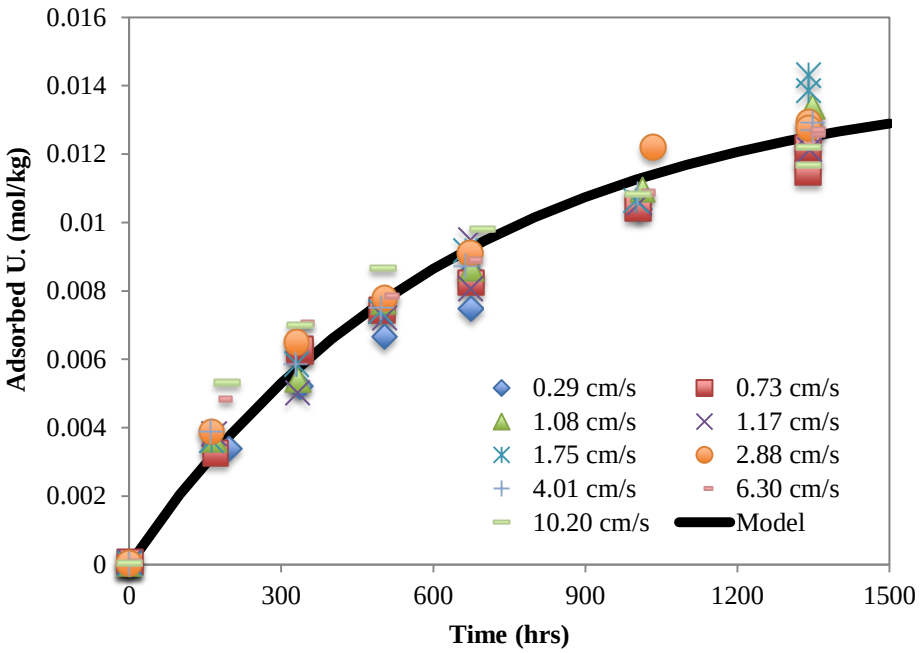

Figure 18. Adsorption uptake data at the various column linear velocities versus modelled using the Reversible Transitional Mechanism reaction-based model and the average optimum kinetic parameters reported in Table 8.

4.3 Flume Experiments

4.3.1 Uranium Time Series Measurements

A summary of the six time series linear velocity experiments conducted using the ORNL AF1 braided adsorbent in a flume exposure is shown in Figure 19. One-site ligand saturation modelling of the time series data shown in Figure 19 is given in Table 10. A comparison of the uranium adsorption capacity for the fastest (5.52 cm/s) and slowest (0.48 cm/s) linear velocity and with one-site ligand saturation modelling curves drawn through the data points is given in Figure 20. There was a higher degree of uncertainty in establishing a one-site ligand saturation modelling curve and modelling parameters for the slowest linear velocity (0.48 cm/s) compared to the other data sets. There was more variability of the data points to the best fit line drawn through the points (see Figure 20), there was higher variability associated with the modelling parameters (see Table 10) and the r-squared value for the curve fitting was 0.78, compared to values of 0.95 or greater for the other curve fitting determinations. Hence, caution should be used in using one-site ligand saturation modelling data for this lowest linear velocity.

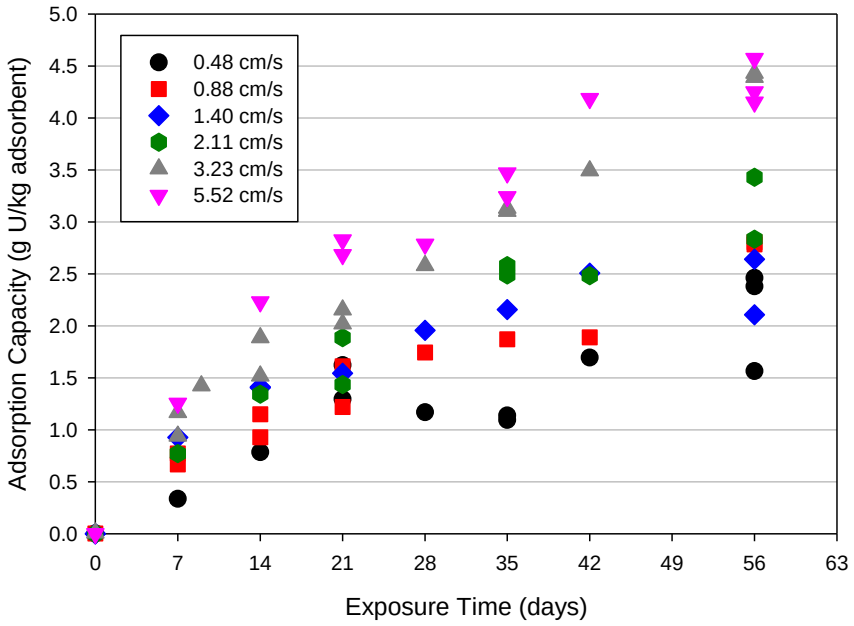

Figure 19. Time series measurements of uranium adsorption capacity at a range of linear velocities using the ORNL AF1 braided adsorbent in a flume exposure. The lower three velocities were conducted in the 8 foot flume (Flume B) and the higher three velocities were conducted in the 6 ft flume (Flume C).

Table 10. One-site ligand saturation modelling of uranium adsorption capacity for the six time series data sets shown in Figure 13.

Linear Velocity (cm/s)	Saturation Capacity[1,2], B_{max} (g U/kg Adsorbent)	Half-Saturation Time[1,2], K_d (days)	56 Day Adsorption Capacity[1,2] (g U/kg Adsorption)
0.48	4.48 ± 2.40	68 ± 58	2.02 ± 1.08
0.88	5.63 ± 1.15	63 ± 20	2.64 ± 0.54
1.40	3.28 ± 0.30	19 ± 4.6	2.45 ± 0.22
2.11	5.90 ± 1.11	50 ± 17	3.11 ± 0.58
3.23	9.51 ± 1.25	69 ±14	4.27 ± 0.56
5.52	6.79 ± 0.62	32 ± 6.3	4.31 ± 0.39

[1] Determined using one-site ligand saturation modelling
[2] Normalized to a salinity of 35 psu

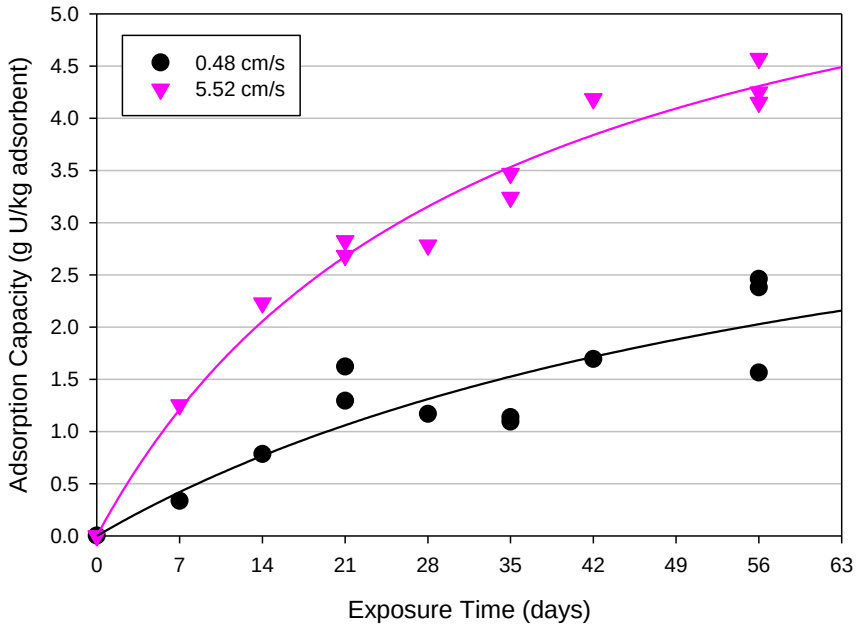

Figure 20. Comparison of the time series measurements of uranium adsorption capacity for the fastest linear velocity (5.52 cm/s) and the slowest linear velocity (0.48 cm/s) with exposure using the PNNL flume. The lines drawn through the data points represent one-site ligand saturation modelling. The modelling parameters are given in Table 9.

The flume tests show a marked uranium adsorption capacity response as a function of the linear velocity of the seawater exposure. With a few exceptions, the faster the linear velocity, the higher the resultant adsorption capacity at all time points in the 56 day exposure period. For example, the 56-day uranium adsorption capacity between the fastest (5.52 cm/s) and slowest (0.48 cm/s) linear velocity exposure varied by more than two-fold (Figure 20 and Table 10). While there is a paucity of data, there appears to be a continual increase in the predicted 56-day adsorption capacity moving from the slowest to the faster velocities until the linear velocity reaches 3.2 cm/s, where the 56-day adsorption capacities for the 3.2 and 5.5 cm/s linear velocities are nearly identical (Table 10). This trend of an increasing adsorption capacity response as a function of linear velocity was also observed at all the other time points as well (Figure 19). The other modelling parameters showed significant variation with linear velocity with no clear trends apparent. Predicted half-saturation times varied from 19 days to 69, and saturation capacities varied between 3.3 and 9.5 g U/kg with no clear trend with linear velocity.

The trend of increasing adsorption capacity with linear velocity and variability in modelling parameters is also consistent with visual observations of the braids appearance during a time series exposure at different velocities (Figure 21)[1]. There is a radical difference between the

[1] There is an implicit assumption here that the intensity and heterogeneity of the color of the braid is reflective of the capacity and heterogeneity of the uranium (as well as other elements and possibly organic compounds) adsorbed on the braid. To date, we do not know what elements or organic compounds are responsible for the color changes that occur as the amidoxime-based adsorbent undergoes exposure to filtered seawater.

color of the braid exposed at the lowest velocity (0.48 cm/s) compared to the fastest velocity (5.5 cm/s). The braid exposed in the fastest velocity quickly darkens evenly throughout the braid, while the braid in the slowest velocity shows a much less intense darkening and much more patchiness in color intensity. The patchiness in color observed in the braid at the lower velocity exposure is consistent with the high variability observed for the lowest velocity time series measurements (Figure 20). Since sampling for the time course measurements involved randomly taking several "snips" off the master braid at each time point, the areas chosen to collect the snips could be from areas with more or less dense color, representing areas with more or less uranium adsorption. This would lead to significant variability in the uranium concentration as was observed for the time course of the braid exposed at the slowest linear velocity.

4.4 Comparison of Flow-Through Column and Flume Exposure Results

A comparison of the one-site ligand saturation modelling results from Tables 3 and 10 obtained using the flow-through column and flume exposure methods is given in Figure 22. There was some general agreement between the results of the two exposure methods, but there were also some notable discrepancies. Any discrepancies between the two test methods cannot be related to different uranium concentrations during different time periods over which the testing was conducted as all the data were normalized to a common salinity of 35 psu.

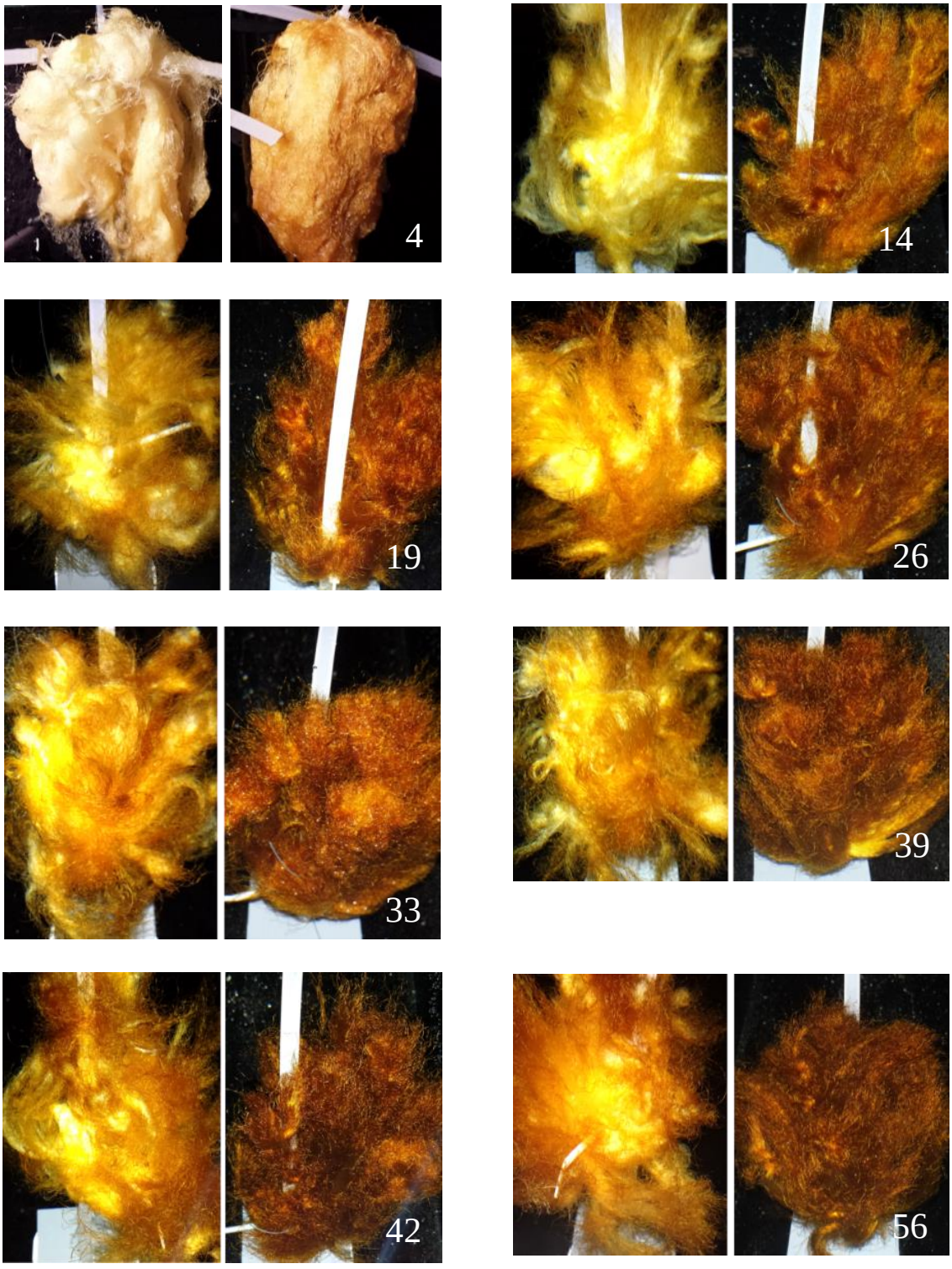

Figure 21. 56-day time series pictures of the ORNL AF1 adsorbent braids during exposure in the PNNL flume. The exposures are grouped in pairs with the slowest velocity on the left (0.48 cm/s) and the fastest velocity on the right (5.52 cm/s). The day of exposure is given by the number in the lower right hand side of the paired pictures.

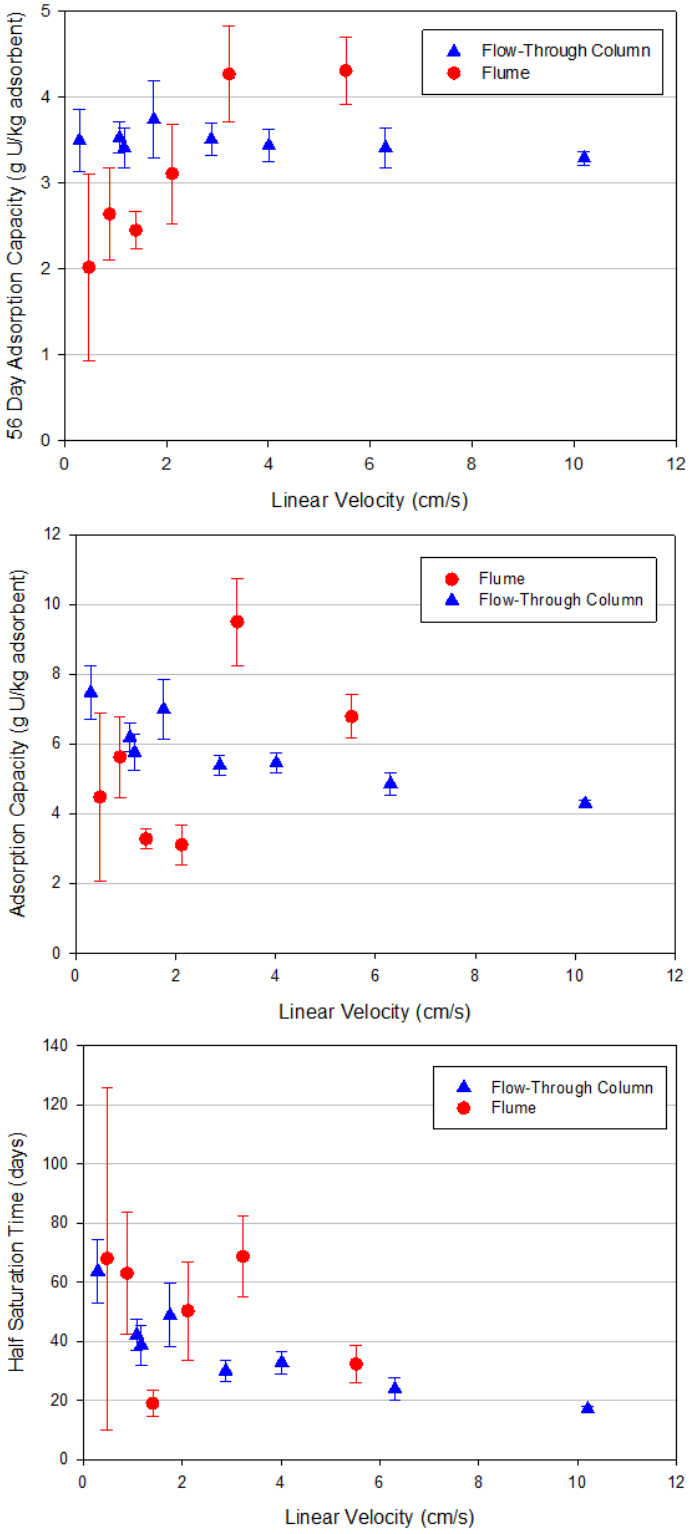

Figure 22. Comprison of one-site ligand saturation modelling parameters as a function of linear velocity for exposures conducted using flow-through columns and flumes.

The flume experiments predicted a significantly higher adsorption capacity at the two higher flume flow-rates (3.23 and 5.22 cm/s, respectively), and lower adsorption capacities at the intermediate linear velocities (1.40 and 2.11 cm/s), than did the column studies. A similar trend was observed for the 56-day adsorption capacities predicted from one-site ligand saturation modelling. The predicted half-saturation times showed a better agreement between the flume and flow-through column exposures, with the exception of the 1.40 cm/s and 3.23 cm/s results obtained in the flume study which were lower and higher than the flow-through column results, respectively. In general, the half-saturation time appears to decrease as linear velocity increases.

Since the adsorbent material that was used for these studies came from a common batch of braids, this implies that the discrepancies observed between the flow-through column and the flume exposures is most likely related to either bias's in the testing methods or the form factor of the adsorbent material (loose fibers vs. braided material) and not due to variations in the adsorption capacity of the material. The exposure that the fibers in the columns experience is a forced flow that individual fibers are exposed to. The exposure the adsorbent experiences in the flume is different, it is an approach velocity represented by a boundary layer surrounding a "clump" of fibers.

4.5 Vanadium Competition

The amidoxime-based adsorbent material is not specific to uranium and adsorbs several other trace elements from seawater, most notably vanadium (Kuo et al., 2015). Hence, it is important to also examine how vanadium competition might influence the adsorption of uranium as a function of linear velocity. Shown in Figure 23 are 56-day time series measurements of vanadium adsorption capacity as a function of linear velocity for the flow-through column and flume experiments. The results obtained for vanadium are very similar to that obtained for uranium (compare with figures 8 and 19). The flow-through column exposures showed less spread in adsorption capacity with time as a function of linear velocity, while the flume exposures had a significant variation in adsorption capacity as a function of linear velocity. The 56-day adsorption capacity for the flow-through column exposures was about 40% higher at the highest flume exposure velocity (5.2 cm/s), compared to the flume exposures. This effect was not observed for uranium.

Time series measurements of the vanadium to uranium (V/U) mass ratio for different linear velocities in the flow-through columns and flume exposures are shown in Figure 24. In marked contrast, the column experiments showed an increase in the V/U with exposure time, while the flume experiments tended to show a decrease in the V/U mass ratio with exposure time. Most interesting is the observation that the V/U ratios in the flume exposure are lower than observed in the column exposure at similar linear velocities. The reason for these discrepancies between the column and flume exposures is unknown, but most likely relates to the different adsorbent form factors of the exposure.

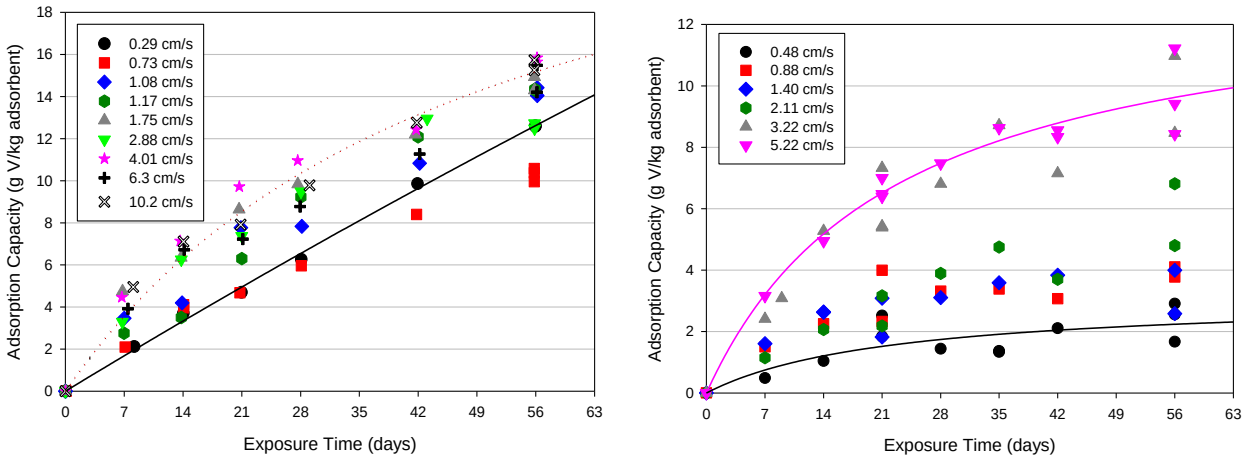

Figure 24. Time Series measurements of vanadium adsorption capacity as a function of the linear velocity of the exposure. The left panel is results obtained with the flow-through column exposure and the right panel is the results obtained for the flume exposure. The lines drawn through the data points represent one-site ligand saturation modelling. Only the fastest and the slowest modelling curves are shown for the flow-through column and flume exposures.

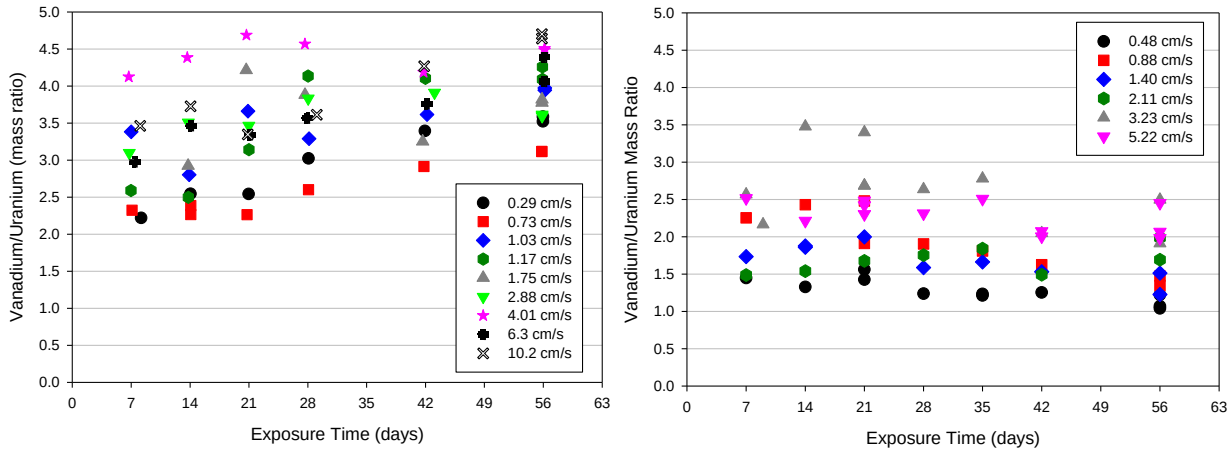

Figure 25. Time series measurements of the vanadium to uranium mass ratio for different linear velocities in the flow-through columns (left panel) and flume exposures (right panel).

5.0 Summary and Conclusions

Analysis of the flow-through column linear velocity data using different kinetic modelling approaches show that linear velocities of the seawater exposure does affect the overall uptake kinetics of adsorption, but only minimally. Linear velocity effects cannot be correlated to any reaction rate constants, since there is no theoretical basis for the relationship between them. Any increases observed in the overall kinetics are most likely caused by an increase in mass transport in the columns and associated increases in interparticle diffusivities. These two mechanisms are directly affected by flow rates and would be responsible for ensuring that plenty of uranium was available to react at the ligand sites on the adsorbent. Having higher uranium fluxes across the fibers results in faster kinetics, because the kinetic reactions are a function of the concentration of available uranium. However, we are unable to quantify how the increases in linear velocity affect column dispersion and mass transport.

Additional analyses or studies need to be conducted to offer an explanation for the differences in adsorbent capacities and other modelling parameters observed between the flow-through column and flume exposure methods. One likely explanation is that the form factor of the adsorbent tested (loose fibers vs. braided adsorbent) plays a significant role in adsorbent capacity and kinetics as a function of linear velocity. Resolving this difference will likely help to develop adsorbent materials with a form factor that optimizes adsorbent capacity and kinetics.

The flume exposure studies show that the linear velocities of 3.23 and 5.52 cm/s produce very similar uranium adsorption capacities and adsorption kinetics. This suggests that at linear velocities above ~ 3 cm/s, there will be minimal improvement in adsorption capacity. However, additional studies that span a larger linear velocity range around this target velocity is needed to confirm this hypothesis.

It is important to note that the flume experiments, which are most representative of exposure conditions in a true marine deployment, were designed to try and minimize turbulence during the exposure using baffles in the tank to force laminar flow. This experimental condition potentially has bearing on the results of a minimum linear flow at which performance no longer increases. At a speed of 3.23 cm/s, the braids in the flume were observed to slowly wave back and forth like kelp or the tail of a kite. At the next slowest velocity (2.11 cm/s), the movement was much slower and with much less range of motion. At the slowest velocities tested (0.48 and 0.88 cm/s) no perceptible movement was observed. These “braid movements”, which are in addition to the linear velocity exposure, likely contributed to the observed adsorbent capacities.

The more important point to take from the observation on braid movements is to design a deployment method that results in producing braid movement. This could easily be engineered into the deployment strategy. For example, using a flexible line at the base of each braid deployment that allowed vertical movement would permit enhanced vertical motion to the entire length of the braid.

6.0 References

Crank, J. (1975). *The Mathematics of Diffusion*, 2nd Ed., Clarendon Press, Oxford.

Das, Sadananda, A. K Pandey, A. A Athawale, and V. K Manchanda (2009). Exchanges of uranium (VI) species in amidoxime-functionalized sorbents. *J. Phys. Chem. B*, **2009**, 113 (18), 6328−6335.

Das, Sadananda, Richard Mayes, Christopher Janke, Li-Jung Kuo, G. A. Gill, J. Wood, and Sheng Dai. Extracting Uranium from Seawater: Promising AF Series Adsorbents. Manuscript submitted to a special edition of *Industrial & Engineering Chemistry Research* on Uranium Separations in Seawater, September 2015.

Gill, Gary A., Li-Jung Kuo, Chris J. Janke, Jordana R. Wood, Richard T. Mayes, Costas Tsouris, Yatsandra Oyola, Jonathan E. Strivens, Michael Cobb , George Bonheyo , Robert Jeters, Jiyeon Park, Tarang Khangaonkar, R. Shane Addleman, Wilaiwan Chouyyok, Marvin Warner , Sonja Peterson, David G. Abrecht, Sadananda Das, Ken Buesseler, Crystal Breier, Evan D'Alessandro, Horng-Bin Pan and Chien Wai. The Uranium from Seawater Program at PNNL: Marine Testing, Adsorbent Characterization, Adsorbent Durability, Adsorbent Toxicity, and Deployment Studies. Manuscript submitted to a special edition of *Industrial & Engineering Chemistry Research* on Uranium Separations in Seawater, September 2015.

Gross, M. G. (1993). Oceanography – A view of Earth. Sixth edition. Prentice Hall, Englewood Hills, NJ, 446p.

Kim, J., Y. Oyola, C. Tsouris, C.R. Cole, R.T. Mayes, J.C. Janke, Dai, S. Characterization of Uranium Uptake Kinetics from Seawater in Batch and Flow-Through Experiments. *Ind. Eng. Chem. Res.*, **2013**, 52 (27), 9433-9440.

Kuo, Li-Jung, Christopher Janke , Jordana R. Wood, Jonathan E. Strivens, and Gary A. Gill (submitted, this volume). Characterization and Testing of Amidoxime-Based Adsorbent Materials to Extract Uranium from Natural Seawater. Manuscript submitted to a special edition of *Industrial & Engineering Chemistry Research* on Uranium Separations in Seawater, September 2015.

Owens, S. A., K. O. Buesseler, and K. W. W. Sims (2011). Re-evaluating the U-238-salinity relationship in seawater: Implications for the U-238-Th-234 disequilibrium method. *Marine Chemistry*, 127 (1-4): 31-39.

Tien, C. (1994). *Adsorption Calculations and Modeling*, Butterworth-Heinemann, Boston.

Wood, Jordana, R., Gary A. Gill, and Key-Young Choe. Matrix Elimination for the Determination of Uranium in Seawater using Inductively Coupled Plasma Mass Spectrometry.

Manuscript submitted to a special edition of *Industrial & Engineering Chemistry Research* on Uranium Separations in Seawater, September 2015.

Pacific Northwest
NATIONAL LABORATORY

Proudly Operated by **Battelle** *Since 1965*

U.S. DEPARTMENT OF
ENERGY

902 Battelle Boulevard
P.O. Box 999
Richland, WA 99352
1-888-375-PNNL (7665)

www.pnnl.gov